TEZ ŞABLONU ONAY FORMU
THESIS TEMPLATE CONFIRMATION FORM

1. Şablonda verilen yerleşim ve boşluklar değiştirilmemelidir.
2. **Jüri tarihi** Başlık Sayfası, İmza Sayfası, Abstract ve Öz'de ilgili yerlere yazılmalıdır.
3. İmza sayfasında jüri üyelerinin unvanları doğru olarak yazılmalıdır. Tüm imzalar **mavi pilot kalemle** atılmalıdır.
4. **Disiplinlerarası** programlarda görevlendirilen öğretim üyeleri için jüri üyeleri kısmında tam zamanlı olarak çalıştıkları anabilim dalı başkanlığının ismi yazılmalıdır. Örneğin: bir öğretim üyesi Biyoteknoloji programında görev yapıyor ve biyoloji bölümünde tam zamanlı çalışıyorsa, İmza sayfasına biyoloji bölümü yazılmalıdır. İstisnai olarak, disiplinler arası program başkanı ve tez danışmanı için disiplinlerarası program adı yazılmalıdır.
5. Tezin **son sayfasının sayfa** numarası Abstract ve Öz'de ilgili yerlere yazılmalıdır.
6. Bütün chapterlar, referanslar, ekler ve CV sağ sayfada başlamalıdır. Bunun için **kesmeler** kullanılmıştır. **Kesmelerin kayması** fazladan boş sayfaların oluşmasına sebep olabilir. Bu gibi durumlarda paragraf (¶) işaretine tıklayarak kesmeleri görünür hale getirin ve yerlerini **kontrol edin**.
7. Figürler ve tablolar kenar boşluklarına taşmamalıdır.
8. Şablonda yorum olarak eklenen uyarılar dikkatle okunmalı ve uygulanmalıdır.
9. Tez yazdırılmadan önce PDF olarak kaydedilmelidir. Şablonda yorum olarak eklenen uyarılar PDF dokümanında yer almamalıdır.
10. **Bu form aracılığıyla oluşturulan PDF dosyası arkalı-önlü baskı alınarak tek bir spiralli cilt haline getirilmelidir.**
11. Spiralli hale getirilen tez taslağınızdaki ilgili alanları imzalandıktan sonra, Tez Juri Atama Formu ile birlikte bölüm sekreterliğine teslim edilmelidir.
12. Tez taslaklarının kontrol işlemleri tamamlandığında, bu durum öğrencilere METU uzantılı öğrenci e-posta adresleri aracılığıyla duyurulacaktır.
13. Tez yazım süreci ile ilgili herhangi bir sıkıntı yaşarsanız, **Sıkça Sorulan Sorular (SSS)** sayfamızı ziyaret ederek yaşadığınız sıkıntıyla ilgili bir çözüm bulabilirsiniz.

1. Do not change the spacing and placement in the template.
2. Write **defense date** to the related places given on Title page, Approval page, Abstract and Öz.
3. Write the titles of the examining committee members correctly on Approval Page. **Blue ink** must be used for all signatures.
4. For faculty members working in **interdisciplinary programs**, the name of the department that they work full-time should be written on the Approval page. For example, if a faculty member staffs in the biotechnology program and works full-time in the biology department, the department of biology should be written on the approval page. Exceptionally, for the interdisciplinary program chair and your thesis supervisor, the interdisciplinary program name should be written.
5. Write **the page number of the last page** in the related places given on Abstract and Öz pages.
6. All chapters, references, appendices and CV must be started on the right page. **Section Breaks** were used for this. **Change in the placement** of section breaks can result in extra blank pages. In such cases, make the section breaks visible by clicking paragraph (¶) mark and **check their position.**
7. All figures and tables must be given inside the page. Nothing must appear in the margins.
8. All the warnings given on the comments section through the thesis template must be read and applied.
9. Save your thesis as pdf and Disable all the comments before taking the printout.
10. **Print two-sided the PDF file that you have created through this form and make a single spiral bound.**
11. Once you have signed the relevant fields in your thesis draft that you spiraled, submit it to the department secretary together with your Thesis Jury Assignment Form.
12. This will be announced to the students via their METU students e-mail addresses when the control of the thesis drafts has been completed.
13. If you have any problems with the thesis writing process, you may visit our **Frequently Asked Questions (FAQ)** page and find a solution to your problem.

☒ **Yukarıda bulunan tüm maddeleri okudum, anladım ve kabul ediyorum. / I have read, understand and accept all of the items above.**

Name :
Surname :
E-Mail :
Date :
Signature : ______________________

COMPARATIVE ASSESSMENT OF THE ROCKING BEHAVIOR OF SEISMIC ISOLATED BRIDGES

A THESIS SUBMITTED TO
THE GRADUATE SCHOOL OF NATURAL AND APPLIED SCIENCES
OF
MIDDLE EAST TECHNICAL UNIVERSITY

BY

POURYA TABIEHZAD

IN PARTIAL FULFILLMENT OF THE REQUIREMENTS
FOR
THE DEGREE OF MASTER OF SCIENCE
IN
ENGINEERING SCIENCES

SEPTEMBER 2021

Approval of the thesis:

COMPARATIVE ASSESSMENT OF THE ROCKING BEHAVIOR OF SEISMIC ISOLATED BRIDGES

submitted by **POURYA TABIEHZAD** in partial fulfillment of the requirements for the degree of **Master of Science** i**n Engineering Sciences, Middle East Technical University** by,

Prof. Dr. Halil Kalıpçılar
Dean, Graduate School of **Natural and Applied Sciences** ________________

Prof. Dr. Murat Dicleli
Head of the Department, **Engineering Sciences** ________________

Prof. Dr. Murat Dicleli
Supervisor, **Engineering Sciences, METU** ________________

Examining Committee Members:

Prof. Dr. Murat Altuğ Erberik
Civil Engineering, METU ________________

Prof. Dr. Murat Dicleli
Engineering Sciences, METU ________________

Prof. Dr. Tolga Akış
Civil Engineering, Atılım University ________________

Date: 06.09.2021

I hereby declare that all information in this document has been obtained and presented in accordance with academic rules and ethical conduct. I also declare that, as required by these rules and conduct, I have fully cited and referenced all material and results that are not original to this work.

Name Last name : Pourya Tabiehzad

Signature :

ABSTRACT

COMPARATIVE ASSESSMENT OF THE ROCKING BEHAVIOR OF SEISMIC ISOLATED BRIDGES

Tabiehzad, Pourya
Master of Science, Engineering Sciences
Supervisor : Prof. Dr. Murat Dicleli

September 2021, 81 pages

In this thesis study a comprehensive roadmap is proposed for detailed modeling of rocking behavior of superstructure deck. Furthermore, a parametric study is conducted to determine effect of the superstructure rocking in enhancing the seismic performance of the box girder type bridge structures. For this purpose, various nonlinear models varying based on one chosen parameter are designed. Nonlinear boundary time history analysis (NTHA) of the models are then conducted being exposed to a set of ground motions scaled with reference to response spectra obtained for a specified coordinate in Canakkale region of Turkey. In the analysis, the effect of different parameters such as number of spans, eccentricity (e) of the bearing lines with respect to pier axis, pier height, span length, friction coefficient of the Friction Pendulum Sliding (FPS) Isolators, radius of curvature of FPS and ground motion scale and intensity are considered. The results of NTHA are then used to discuss the effects of these parameters on the seismic performance of box girder bridges in terms of pier moment and base shear.

. Keywords: Seismic Isolation, Parametric Study, Rocking of Superstructure

ÖZ

DEPREM YALITMLI KÖPRÜLERİN SALINIM DAVRANIŞININ KARŞILAŞTIRMALI İRDELENMESİ

Tabiehzad Pourya
Yüksek Lisans, Mühendislik Bilimleri
Tez Yöneticisi: Prof. Dr. Murat Dicleli

Eylül 2021, 81 sayfa

Bu tez çalışmasında, köprü üst yapı salınım davranışının detaylı modellenmesi için kapsamlı bir yol haritası önerilmiştir. Ayrıca köprü salınım davranışının, kutu kiriş tipi köprülerin sismik performansını iyileştirmede oyanıdığı rölü irdelemek adına parametrik bir çalışma yapılmıştır. Bu amaçla, seçilen her parametreye göre değişen çeşitli köprü modelleri tasarlanmıştır. Modellerin Türkiye'nin Çanakkale bölgesinde belirli bir koordinat için elde edilen tepki spektrumlarına göre ölçeklenen bir dizi yer hareketi altında zaman tanım alanında doğrusal olmayan analizleri yapılmıştır. Analizlerde, köprü açıklık sayısı, köprü mesnetlerinin köprü ayak eksenine mesafesi, köprü ayak yüksekliği, köprü açıklık uzunluğu, sürtünmeli sarkaç mesnetlerin sürtünme katsayısı, sürtünmeli sarkaç mesnetlerin eğrilik yarıçapı, yer hareketi şiddeti gibi farklı parametrelerin etkisi incelenmiştir. Zaman tanım alanında doğrusal olmayan analizlerin sonucu daha sonra, belirlenen parametrelerin kutu kesitli köprülerin sismik performansı üzerindeki etkilerini, ayak momenti ve ayak kesme kuvveti açısından ele almak için kullanılmıştır.

.Anahtar Kelimeler: Sismik İzolasyon. Parametrik Çalışma, Köprü Salınımı

Dedicated to my Parents

ACKNOWLEDGMENTS

First of all, I would like take this opportunity to express my deepest gratitude to my supervisor Prof. Dr. Murat Dicleli for all his guidance, advice, constructive criticism, and encouragements throughout this research. He was not just an academic advisor but also a life-changing teacher who taught me how to discipline myself and have an organized mindset in achieving my goals. It was an honor for me to find a chance to work under his supervision.

I would also take this chance to thank Dr. Mümtaz Kibar for all his positive role and support which he provided me at different aspects of my life.

I would also like to thank my friends Mr. Sezer Mutlu, Mr. Çağrı İmamoğlu and Mr. Oğuz Alp Taçyıldız for all their support and friendship during my study.

I would like take this especial chance to thank Ms. Tannaz Mohammadi for her unconditional support during all my difficult moments. Her continuous support, motivation, as well as her positive approach towards finding solution to problems has helped for me from the first moment of this study. I am grateful for all her positive role and energy.

I would like to send an especial thanks to my lovely aunt for her endless care during all my past years of university life. She taught me the meaning of generosity and sacrifice.

Last but not least, I would like to thank my kind father and mother for their endless love and trust in me and for the light which they are true reason for, in my life. I could not imagine a lifetime without their vision and their full unconditional support and care. They are truly the gift of life for me.

TABLE OF CONTENTS

LIST OF TABLES

TABLES

LIST OF FIGURES

FIGURES

CHAPTER 1

INTRODUCTION

The improtance of Siesmic Isolation as a protective method in improving the performance of the structures is becoming popular day by day and as a spesific type of mechanisim, structure protection systems are also widely considered in design of the bridges, Friction Pendulum type of bearing isolators are among the most preferred systems in their own category and their application and usage is spreading fastly especially at countires which are under high risk of ground motion excitation like Turkey.

The scope of this research study is limited to Straight Box-Girder pre-stressed concrete highway bridges with no skew. The abutments at both end of the bridge are considered to be designed identical to each other and are assumed to have full contact with the backfill soil. Furthermore, with the aim of simulation of foundation ground, dense soil and soil rock is used considering the ground soil composition of the Canakkale region.

In order to study the seismic performance of bridges as a function of various structural parameters, a three span benchmark bridge is considered. Bridge location and girder chosen are from real life example currently under construction in Turkey which is designed by an engineering company currently providing consultation service for the viaduct designs of KINALI - TEKİRDAĞ - ÇANAKKALE - SAVAŞTEPE MOTORWAY PROJECT located in Turkey. The geographical conditions and the design methodology of the bridge is consistent with the hypothesis of this study to be subject to investigation to understand the bridge deck rocking phenomena. In doing so, various three dimensional (3D) nonlinear structural models are built through changing one chosen parameter at each set of analysis using the MIDAS CIVIL, highly developed engineering software. For all of the generated models, seismically isolated bridge design inholding friction pendulum type of sliding isolator bearing is done with reference to (AASHTO Guide Specification for Seismic Isoaltion Design, 2014) . The embedded footing dynamics are reflected with reference to a study by George Gazetas in handling the soil–foundation interaction under the effect of the applied dynamic loads. For the case of the abutment-backfill interaction, the effects of backfill soil pressure together with backfill shear strength factors, both are represented in building structures of the models through a stepwise detailed approach discussed later under the modeling section. The Simple Rocking Motion (SRM) proposed by (Housner, 1963) is used to define a rocking motion of superstructure. The relation between coefficient of restitution and damping ratio is also obtained with reference to a distinctive approach available in literature to figure out amount of energy dissipated during rocking and contact of bodies. The boundary nonlinear time history analysis of the structural models is then conducted under dynamic effect of scaled set of ground motions obtained from Pacific Earthquake Engineering Research Center (PEER) ground motion database with reference to design spectra of a specific coordinate marked for motorway viaduct in Canakkale region of Turkey. During the analysis, the effect of various structural parameters on the rocking behavior of the bridge is investigated through varying quantities appointed to parameters namely, number of spans, eccentricity (e) of the bearing lines with respect to pier axis, pier height, span length, friction coefficient of the Friction Pendulum Sliding (FPS) Isolators, radius of curvature of FPS Isolators and applied ground motions' intensity. Finally, the seismic performance of models is discussed through a comparative approach in terms of maximum pier moment, maximum pier base shear and axial loads exerted on FPS Sliding bearings located above critical piers. All the obtained outcomes prepared a framed ground in deciding for the structural aspects of the models being designed to undergo a rocking motion as an applicable mechanism with the aim of improving seismic performance of the box girder highway bridges.

CHAPTER 2

LITERATURE REVIEW

Conventional Seismic design of RC structures considers ductile behavior of the structure in order to prevent brittle failure of the structure by tolerating damage in some acceptable range through the formations of flexural hinges in overall system (i.e. for the case of bridges, top and/or bottom of piers experiencing plastic hinge formation) (Alessandro Palermo, Stefano Pampanin, Gian Michele Calvi, 2004). Recent developments in the area of passive seismic protective systems has shifted the tendency of engineers from capacity seismic design type of approach towards designing systems showing fully elastic response under the effect of ground motions. Seismically isolated structures and structures showing a rocking behavior are all among this category.

Structural rocking has been a popular phenomenon in the last decade for research studies to understand it's effect on performance of the structures subjected to the ground motion excitations. In early 1960s, Housner studied the rocking behavior of idealized rigid blocks and found that due to an scale effect, geometrically similar but larger of the two blocks shows better stability under the effect of seismic excitation; additionally, he also revealed that, despite the general expectation about tall slender blocks' behavior deduced from their behavior under constant horizontal force, they tend to have much greater stability under seismic effect (Housner, 1963). This study has been followed by various research studies all around the world in an attempt to better figure out the dynamics associated with the phenomenon from analytical and experimental point of view by considering different aspects of the matter with having a fixed focus on the structural performance (Chik-Sing Yim, Anil K. Chopra And Joseph Penzien, 1980) (Jennings, Ioannis N. Psycharis And Paul C., 1983)

(Makris, Jian Zhang and Nicos, 2001). (R. H. Plaut, W. T. Fielder and L. N. Virgin, 1995) , (Makris, 2014) , (Sivapalan Gajan , Duraisamy S.Saravanathiiban) (Iason Pelekis, 2017). Glancing at the findings within the context of rocking and its effectiveness in application to bridges, we can see that, several ideas has been proposed by researchers taking into account different aspect of the context. Concept of rocking of piers is among these ideas raised (Athanasios Agalianos, 2017). In this sense two distinct approaches are available in the literature. The first approach has root in the concept of controlled rocking (John Stanton, 1997) (Dimitrios Kalliontzis, 2019) (Priestley MJN, 1999) and considers a restraining tendon used to enable the re-centering of the pier at the end of each phase of motion to acquire stability of the structure (J.B. Mander and C-T.cheng, 1997); (Alessandro Palermo, Stefano Pampanin, Gian Michele Calvi, 2004); (Yi-Hsuan Chen, 2006); (Cheng, 2008) (Dion Marriott1, 2009); (Nicos Makris, 2014); (Michalis F. Vassiliou and Nicos Makris, 2015); (Dimitrakopoulos, 2017). Other approach, takes into account rocking of piers which are allowed to rock without tendon like the case for South Rangitikei Bridge in New Zealand designed in 70's (J. L. Beck and R. I. Skinner, 1973). The former approach also has been implemented during the design of Wingram-Magdala link Bridge (R. Liu & A. Palermo, 2016) (P.J. Routledge, M.J. Cowan, A. Palermo). Additionally, there is another concept known as Footing Rocking (Athanasios Agalianos, 2017). In implementation of this mechanism, through under-sizing the foundation blocks on purpose, it is being tried to promote full mobilization of their moment capacity during seismic shaking. In this manner, during the seismic excitation, the soil underlying the foundation undergoes an inelastic kind of response and allows uplift of the footing (e.g., (Panagiotis Elia Mergos, Kazuhiko Kawashima, 2005); (Kutter, Sivapalan Gajan and Bruce L., 2008); (I. Anastasopoulos, G. Gazetas, M. Loli, M. Apostolou, N. Gerolymos, 2010); (F. Gelagoti, R.Kourkoulis, I.Anastasopoulos, G.Gazetas, 2012) (Grigorios Antonellis, Andreas G. Gavras, Marios Panagiotou, Bruce L. Kutter, Gabriele Guerrini, Andrew C. Sander, Patrick J. Fox, 2015). For the context of the bridges, unlike the substructure and foundation rocking, the uplift and rocking of the superstructure has not been in depth analyzed; In most of the real cases, superstructure uplift has been prevented by adding uplift restrainer devices and despite the high cost of implementing these type of restraining devices, still engineers tend to get use of this approach claiming that, there is possibility of deck unseating and pounding between different segments of the bridges like bearing and abutment and this leads to have risk of damage and through this argument they support usage of such devices in better control of undesired outcomes (Bipin Shrestha, 2016). There is a strong possibility of rocking behavior and uplift of the deck in the case of highway pre-stressed concrete box girder bridges having a limited eccentricity between their bearings and their pier axis. In this context, the effect of the superstructure deck rocking and the advantages or disadvantages of free rooking and uplift of the deck is still question mark and may depend on several factors and parameters addressed for the scope of the study.

Accordingly, this research study aims to investigate the effect of various structural and geometrical properties and parameters on the seismic performance of the Highway Box Girder Bridges and during the study it's been tried to propose a guidance and framework for modeling and simulation of the superstructure deck rocking. It has been tried to propose a mechanism through using some sort of fictitious dampers to estimate the amount of energy dissipated as a result of the contact being occurred among bodies. To this end, results of this parametric study are used to establish a logic in handling the phenomenon of the superstructure rocking and its effect on seismic performance of the bridges. Bridge design engineers and researchers may then get use of the results and outputs of this study in handling the rocking or isolation rocking aspect of their future works.

CHAPTER 3

DESCRIPTION OF THE BENCHMARK BRIDGE AND PARAMETERS CONSIDERED IN THIS STUDY

A three span seismically isolated box girder highway bridge located in Canakkale region of Turkey is considered to investigate the effect of multiple parameters on the rocking behavior of bridge deck superstructure and from a more general perspective, on the seismic performance of the bridge.

The benchmark bridge has a total length of 150 m and its width is 17.50 m (Shown at Fig.1 and Fig.3). Moment of inertia of the deck cross section is 25.36 m^4 about transverse axis and 31.45 m^4 about longitudinal axis. The bridge has three spans with lengths of 50 m each. The bridge deck is continuous from one abutment to the other and is composed of single cell box. The bridge pier is composed of box section with cross section dimensions of $4{\times}6\ \mathrm{m}^2$, wall thickness of one meter from both sides and height of 30 m which supports a cap beam with $9.40 \times 5.5\ \mathrm{m}^2$ dimensions and a thickness of 2 m . The abutments of the benchmark bridge are 11 m tall, with 18 m width and 2 m wall thickness supporting friction pendulum type of sliding isolator bearings. The dimensions governing the design of sliding bearings related to the material used and geometry of sliding surface are friction coefficient μ, chosen to be 0.04, and radius of curvature R, chosen to be 5 m. The other important factor in considering FPS system is design displacement, D chosen to be 40 cm. For the benchmark bridge under consideration, isolators' stiffness value at abutment-deck connection phase are different from the stiffness values obtained for the isolators above piers due to difference at axial load being exerted to isolators due to the dead load of deck. The bridge is founded on ground type C according to ASCE/SEI 7-10. The foundation dimensions chosen for piers are $20 \times 30\ \mathrm{m}^2$ with thickness of 3.5

m. The peak ground acceleration used in design of benchmark bridge is equal to 0.7 (g).

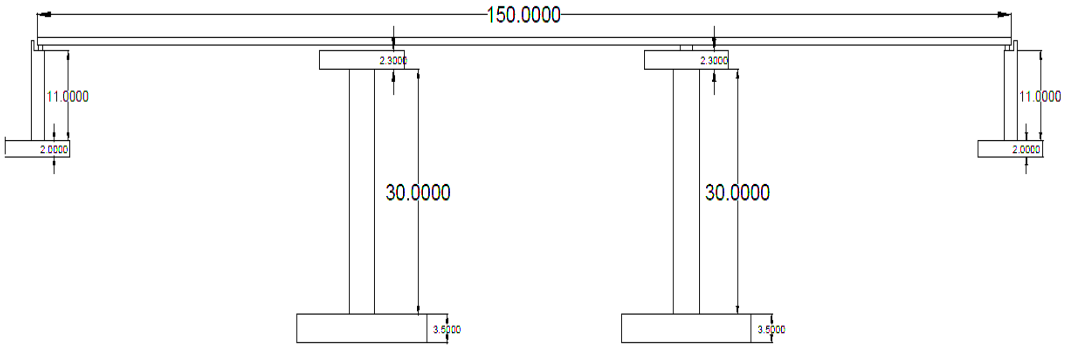

Figure .1 Elevation view of Benchmark Bridge Considered for the Purpose of Study

Figure 2. Bridge Pier Cross Section

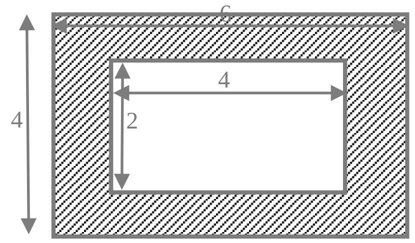

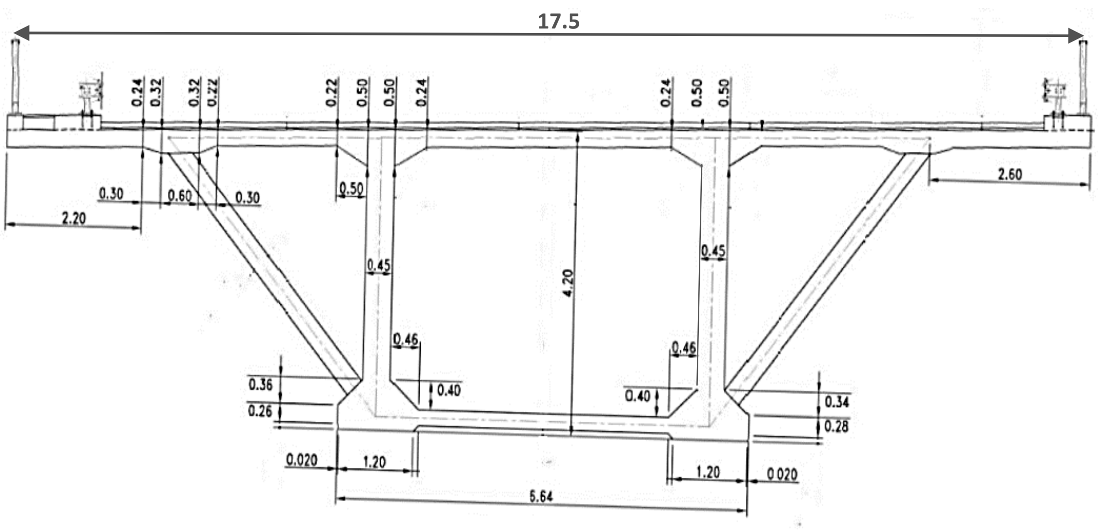

Figure. 3 Bridge Deck Cross Section

For the parametric study, the number of spans is anticipated to affect the seismic behavior of bridges. Therefore, 5 different span number values (2-spans, 3-spans, 4-spans, 5-spans, and 6-spans) are considered for the analysis. In addition, to understand the effect of distance between each set of bearings on the seismic performance of the bridges, five different values (3.4, 4.4, 5.4, 6.4, and 7.4 m) are considered for the analysis. To investigate the effect of pier height on the seismic behavior, three different pier heights (20, 30, 40 m) are considered. Furthermore, to assess the effect of span length on seismic performance of bridge in association with rocking behavior, five different values (30, 40, 50, 60, and 70 m) are chosen. Moreover, to understand the effect of different characteristics of Friction Pendulum Sliding, the analysis are repeated by taking into account five different friction coefficient values (0.02, 0.03, 0,04, 0.05, and 0.06) and five different FPS radius of curvature values (3, 4, 5, 6, and 7). Top all, to clearly observe the seismic performance difference in both cases of Uplift-Allowed and Uplift-Restricted models, different ground motion intensities determined based on various peak ground acceleration values are chosen to be considered for the analysis. The parameters chosen to be subject of investigation at this study are reflected in Table 1.

Table 1 . Paramters Chosen For the Aim of Study

Parameters	Description
Number of Spans	2, 3, 4, 5, 6
Distance between Bearings (m)	3.4, 4.4, 5.4, 6.4, 7.4
Span Length (m)	30, 40, 50, 60, 70
pier Height (m)	20,30, 40
FPS Friction Coefficient	0.02, 0.03, 0.04, 0.05, 0.06
FPS radius of curvature (m)	3, 4, 5, 6, 7
Peak Ground Acceleration values (g)	0.35, 0.7,1.05, 1.4, 1.75

CHAPTER 4

ROCKING PHENOMENON AND ASSOCIATED ENERGY DISSIPATION

Free-standing rocking of a rigid block can be explained as the rotational movement of unrestrained body with respect to its underlying base (Housner, 1963) . Rocking behavior of free-standing bodies which is the foundation stone of the rocking analysis and the basis for researchers to understand the type of the motion and its mechanism, has been extensively analyzed in different studies. In this study it has been tried to create an analogy between the behavior of the bridge deck in transverse direction and the behavior of the simple rocking model which was initially developed by (Housner, 1963) to analyze the rocking phenomenon.

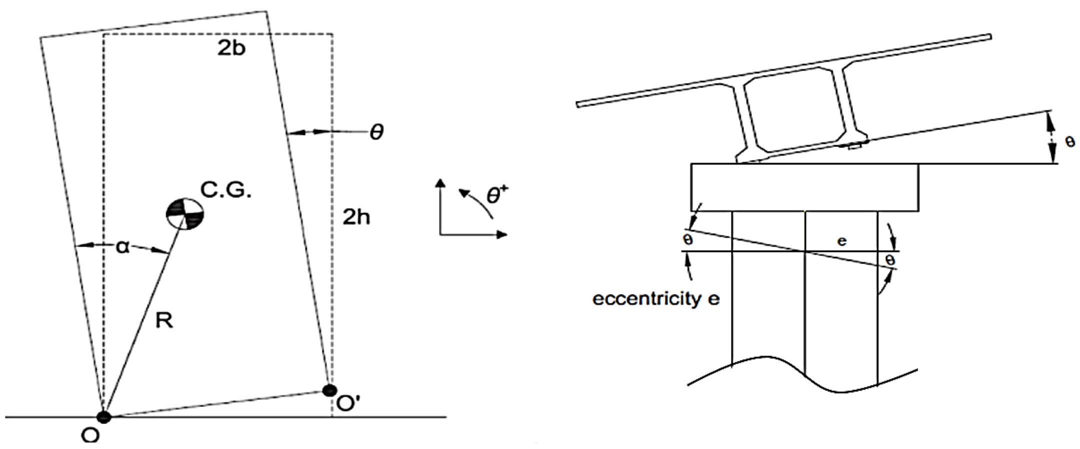

Figure. 4 Free body Diagram of Rocking Body Together with Cross Section of the Rocking Superstructure or Bridge Deck

4.1 Standing Rocking Motion of the Superstructure

First of all, it has been tried to simulate the behavior of bridge deck during rocking by its similarity with dynamics of free-standing rocking body. As a result of this similarity, all involved parameters are calculated with reference to free-standing rocking block geometric properties. In the following paragraph the nature of this shared behavior has been explained in detail. In the case of simple rocking motion considered for rigid block, When θ is approaching 0, the block impacts with its foundation, while reducing its kinetic energy. After impact, rotation of the block continues with respect to its opposite bottom corner. We can apply the same analogy in analyzing the behavior of the bridge superstructure supported on seismic isolator bearings. Under the excitation of ground motion, bridge deck rocks with respect to one of the corners of its girder box, the angle of the rotation is called θ similar to the case for free-standing rigid block. Following the uplift of one of the corners, when θ approaches zero, the impact occurs between the bottom layer of the isolator and the deck. As a result of the contact, the body's kinetic energy is being reduced and in the following phase, bridge deck rocks and rotates about the opposite corner repeating the same behavior. (Housner, 1963) explained the free vibration response of the Simple Rocking Motion (SRM) by Equation (1) as follows:

$$I_0\ddot{\theta} + MgRsin[sign(\theta)\alpha - \theta] = 0 \quad (1)$$

Table 2. Parameter Description of Free Vibration Response of the SRM.

Parameter	***Description***
Io	Mass moment of inertia with respect to its bottom corner
M	Mass of the rocking motion body
R	Distance between its center of gravity and the bottom corner
$\boldsymbol{\alpha}$	Degree of slenderness of the rocking body
$\boldsymbol{sign(\theta)}$	Sign of rotational direction
$\boldsymbol{sign(\theta)}$	$\theta > 0 \rightarrow 1$ $\theta < 0 \rightarrow -1$

The equation (1), was changed to linear one by Housner for the cases when $\alpha < 20°$.

$$I_0\ddot{\theta} + MgR[sign(\theta)\alpha - \theta] = 0 \tag{2}$$

Using this new equation , Housner computed a closed-form solution for $\theta(t)$ using the initial conditions of $\theta = \theta_0$ and $\dot{\theta} = 0$. This solution is reproduced in following Equation (3) as follows:

$$\theta(t) = \alpha - (\alpha - \theta_0)coshpt. \tag{3}$$

Where $P = \sqrt{MgR}/I_0$ (4)

Getting use of the approach explained above and (Housner, 1963)'s further estimations in using coefficient of restitution approach, the reduction in kinetic energy of the rocking body at impact for bridge deck superstructure can be obtained by equation (5). It was assumed that conservation of angular momentum between the moments just before and just after an impact holds with respect to the rotation center of the body just after the impact. Accordingly, *CR* is as follows (Dimitrios Kalliontzis, 2019) :

$$CR = (\frac{\dot{\theta}_2}{\dot{\theta}_1})^2 = [1 - \frac{MR^2}{I_0}(1 - COS(2\alpha))]^2 \tag{5}$$

4.2 The Relation Between Coefficient of Restitution and Damping Ratio

Structural Pounding as a result of the ground motion excitation is an important factor which needs an extra attention from performance and serviceability point of view. Phenomena of rocking may result in pounding at the moment of the impact. In order to take Pounding into consideration, a linear viscoelastic impact element (spring-dashpot) is introduced between the masses which acts only during the approach period of them.

Especial Impact element which consists of spring and dashpot is being considered in investigation of collision between two structures during earthquake and the general formula to mathematically summarize the impact force model is noted down here as Equation (6) (Jankowski & Mahmoud, 2015) (Seyed Mohammad Khatami, Hosein Naderpour , Rui Carneiro Barros ,Anna Jakubczyk-Gałczynska, and Robert Jankowski, 2019). Different approaches for impact damping ratio, in relation with *CR*, are used by a number of researchers. In this regard, based on the logic presented by (Anagnostopoulos, 1988), (Rui C. Barros, H. Naderpour, S.M. Khatami, and A. Mortezaei, 2013), the interaction of adjacent SDOF systems shown in Figure 5 colliding with each other is considered and as a result of this collision a hysteretic response which can be taken into account in calculation of kinetic energy dissipation, is obtained. *CR* as a role-playing parameter takes value between 0 (fully plastic) and 1 (fully elastic). The relation obtained at equation (9) was based on the assumption of an equivalent SDOF dynamic system representing two bodies in contact and the fact of conservation of energy before and after impact (Rui C. Barros, H. Naderpour, S.M. Khatami, and A. Mortezaei, 2013).

$$F_{imp}(t) = k_s \delta^n(t) + c_{imp}\dot{\delta}(t) \tag{6}$$

$$c_{imp} = 2\xi_{imp}\sqrt{K_S M_{eq}} \quad \text{(linear Models)} \tag{7}$$

$$M_{eq} = \frac{m_d m_p}{m_d + m_p} \tag{8}$$

$$\xi_{imp} = \frac{-\ln(CR)}{\sqrt{\pi^2 + (\ln(CR))^2}} \tag{9}$$

k_s: Stiffness of the substructure

Table 3. Parameter Description of Impact Damping Model

Parameter	Description
Power of n	Equals to 1 (linear models)
$\mathbf{k_s}$	Impact stiffness
$\mathbf{m_d}$,$\mathbf{m_p}$	Masses of colliding bodies respectively
$\boldsymbol{\delta}^{\mathbf{n}}(\mathbf{t})$	Relative Displacement
$\dot{\boldsymbol{\delta}}(\mathbf{t})$	Relative velocity
$\boldsymbol{ln}(\boldsymbol{CR})$	Natural logarithm of CR

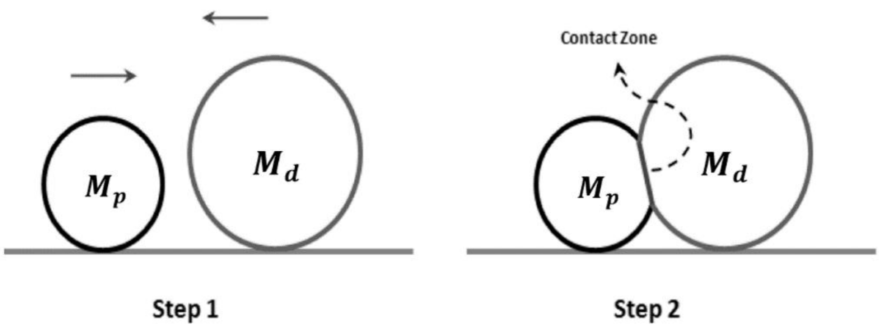

`Figure 5. Schematic Model of Impact Between Two Adjacent Masses

CHAPTER 5

MODELING OF BRIDGE

In order to investigate the effect of various structural parameters on the performance of the Box Girder Bridges, 3D bridge model is chosen to figure out the correlation existing among rocking behavior of superstructure and different governing parameters.

The bridge superstructure deck is modelled using a 3D beam elements having a C45/50 concrete as specified material type. The cross section assigned for the beam members of the superstructure, namely the deck cross section is shown in the Fig. 3.

The reinforced concrete cap beam and piers underneath are modeled as 3D beam elements having C40/45 concrete as specified material type. Since the scope of the study focuses on the performance of seismically isolated bridges, there is no possibility of plastic hinges to be occurred at the pier top or bottom; piers will remain in their elastic range. The cross section of the piers is shown in Fig. 2.

As indicated, the rocking response of all designed bridges for this study are analyzed under transverse response. Various modeling features of the program such as Point Springs, Elastic Rigid Links, Force and Element Type General Links facilitated the simulation of the bridges' behavior such as nonlinear and hysteretic behavior of structural members like bearing isolators as well as linear behavior of the foundation-soil interaction. In the following subsections, details of these 3D nonlinear structural models are presented.

5.1 Modeling of Bearings and Isolation System

The isolator bearings considered for this study are Friction Pendulum Sliding (FPS) type of bearings. Two major characteristics of this type of bearings are their sliding motion on the curved surface and their idealized hysteretic behavior (Murat Dicleli, Jung -Yoon LEE and Mohamad Mansour, 2004) shown in Fig. 6.

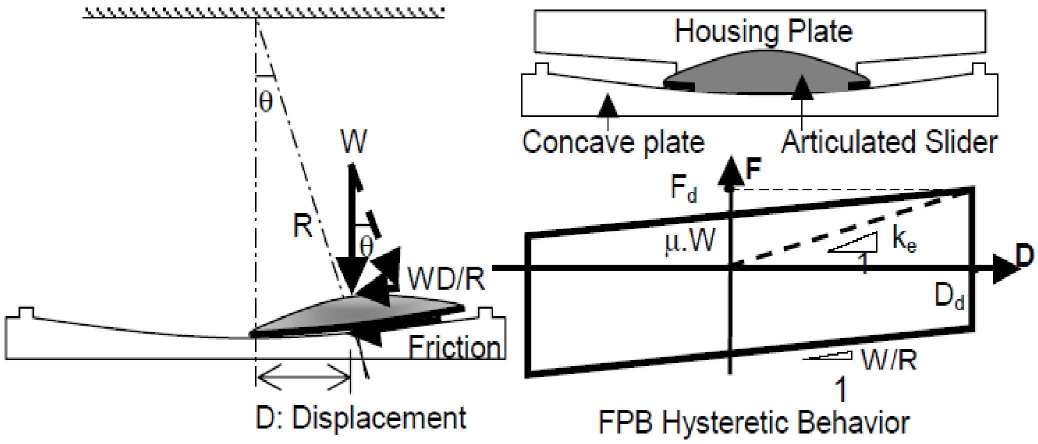

Figure 6. Behavior of Curved Sliding Bearing and it's Bilinear Idealized Hysteretic curve

5.1.1 Equivalent Linear Method Considering Simplified Method Approach Described at AASHTO Guide Specification for Seismic Isolation Design

At the first stage to design the isolation system and specify the specific characteristics of the isolators, a simplified method is adopted, that is as follows:

1. An approximate design displacement is chosen
2. Depending on the chosen value of design displacement, the effective stiffness value is calculated using the following formula:

$K_{eff} = \frac{\mu \times W}{D} + \frac{W}{R}$ Effective Stiffness of The Bearing Isolator

μ	Friction Coefficient
W	Total Vertical Load Applied on The Isolator Bearing
D	Design Displacement
R	Radius of Curvature

The corresponding total stiffness and equivalent damping ratio of the isolation system shall be determined as follows (AASHTO Guide Specification for Seismic Isoaltion Design, 2014):

$K_{effj} = \dfrac{K_{Sub} \times K_{eff}}{K_{Sub} + K_{eff}}$ Total stiffness of the Bearing isolator together with the substructure underlying

K_{Sub}	Stiffness factor depicted for substructure unit
K_{eff}	Effective stiffness of the bearing isolator

In the benchmark bridge, two different K_{eff} values are used for the isolators because of the difference in the existing dead load due to the weight of the superstructure (deck) in the connection interphase of the superstructure and substructure.

$K_{eff\,Total} = \sum K_{effj}$ Total isolation system stiffness

3. **Equivalent** total viscous damping of the isolation system is calculated based on following formula

$\xi = \dfrac{2\sum[Q_d(d_i - d_y)]}{\pi\sum\,[K_{effj}(d_i + d_{sub})^2]}$ Equivalent viscous damping ratio of the isolation system

d_y: Yield Displacement (taken as zero in the current case)

d_i: Displacement of Isolator Unit

d_{sub}: Zero in this case

Q_d: Characteristic strength of isolator unit which equals to $\mu \times W$

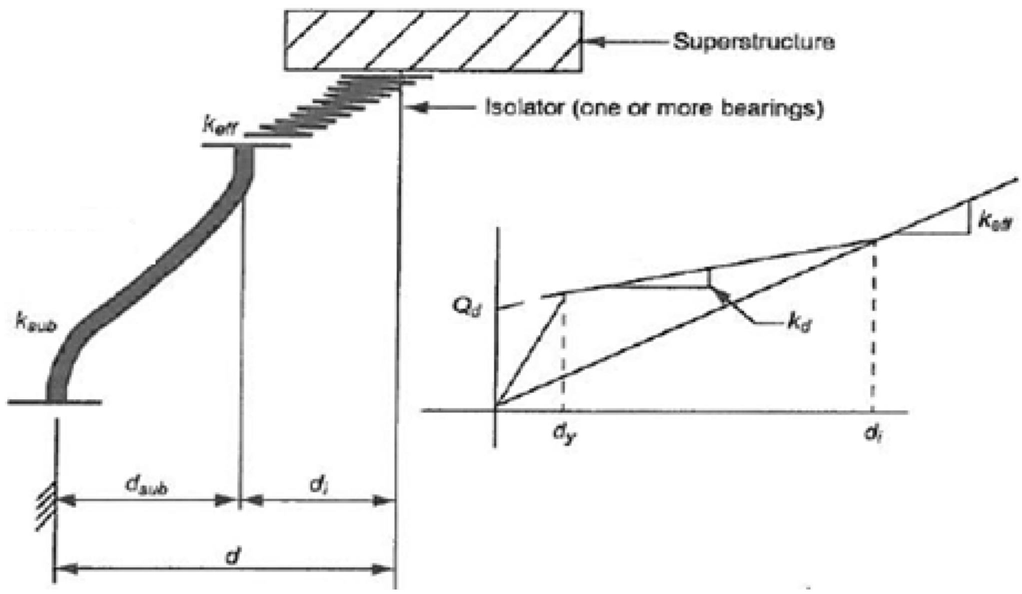

Figure 7. Sliding Isolator and Substructure Deformations Due to Lateral Load

4. Following the calculation of viscous damping value, the reduction factor B_L is calculated accordingly:

   $B_L = (\frac{\xi}{0.05})^{0.3}$

5. Meanwhile the isolation mode period of the structure T_e is being calculated having the total mass and total isolation system effective stiffness values. The accuracy of the value is checked by comparing with eigenvalue analysis outputs of MIDAS Civil program as well.
6. Using the B_L factor, the acceleration values of target spectrum are being reduced in order to account for the effect of isolation system existence in the structure. To do so, $0.8\times T_e$ is calculated and the range of acceleration data greater than $0.8\times$ Te are being reduced , through division by B_L factor.
7. New analysis run is carried out; then, displacement values D_{i+1} obtained from Midas Civil program analysis results are compared with initially assumed value of design displacement.

8. This iteration-based loop is repeated till making the D_{i+1} approximately equal to D_i

For the benchmark bridge considered in current study the values specified for isolator's design displacement is 0.4 m

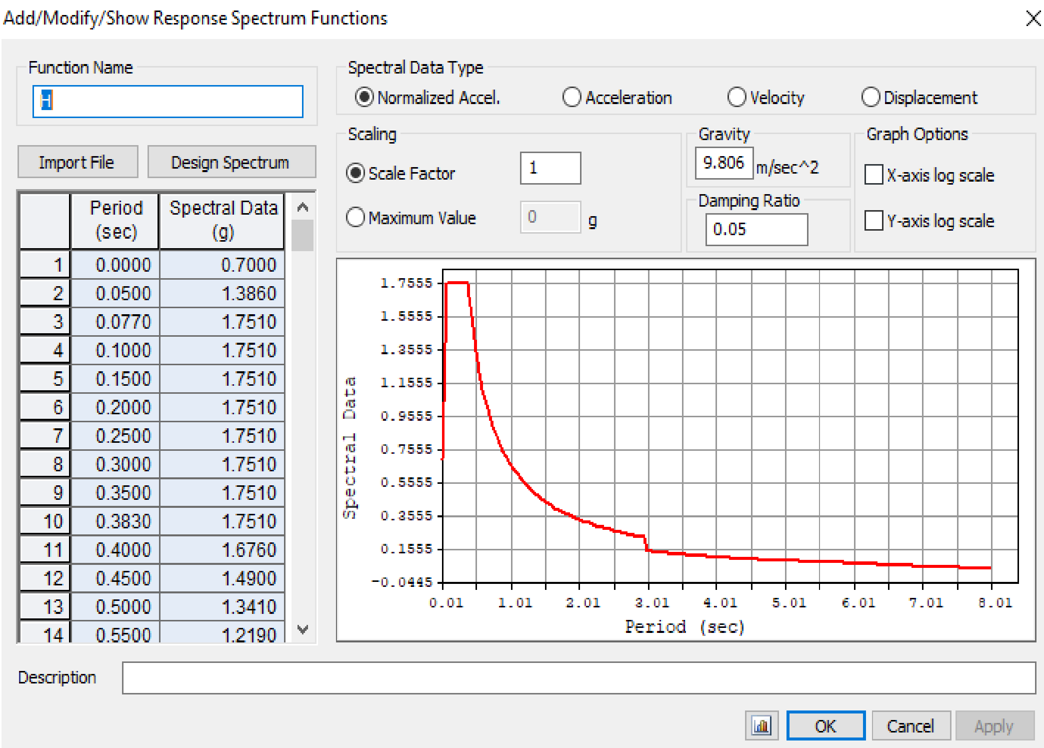

Node	Mode	UX	UY	UZ	RX
EIGENVALUE ANALYSIS					
	Mode No	Frequency (rad/sec)	(cycle/sec)	Period (sec)	Tolerance
	1	1.687107	0.268511	3.724236	0.0000e+000
	2	1.697377	0.270146	3.701704	0.0000e+000
	3	1.752309	0.278889	3.585660	0.0000e+000
	4	9.848746	1.567477	0.637968	0.0000e+000

Figure 8. Reduced Response Spectrum and Isolation Modes' Period obtained from Midas Civil

5.1.2 Nonlinear Boundary Time History Analysis and Associated Parameters

By using the Isolation modes' periods of the bridge structure, the mass proportional constant of the Rayleigh damping equation can be calculated accordingly by using the following formula:

- Mass Proportional Coefficient:

$$\frac{2 \times \xi \times 2\pi}{T} = \frac{2 \times 0.02 \times 2\pi}{3.7} = 0.0679$$

- Stiffness Proportional Coefficient:

0.0002

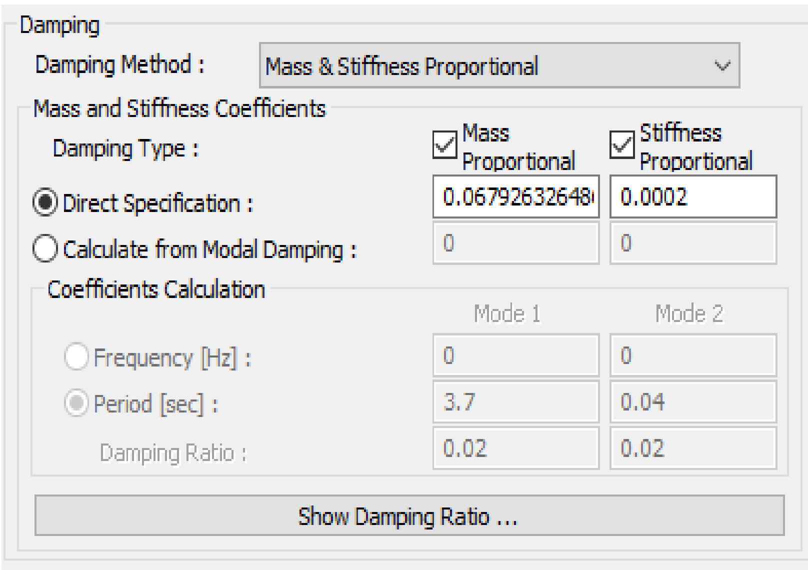

Figure 9. Mass and Stiffness Coefficients of Rayleigh Damping Equation Entered to Program

Axial Spring Stiffness value of bearing isolators considered for benchmark bridge: Midas Civil program default defines axial spring property of FPS as gap type spring; in other words, FPS system under axial load behaves as compression only link.

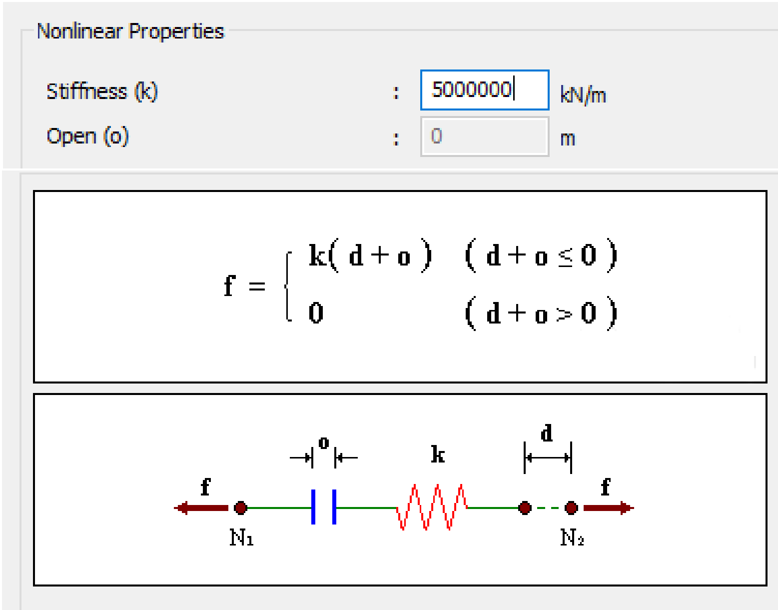

Figure 10. Axial Spring Property of FPS Bearing

Shear Springs Stiffness value of bearing isolators considered for benchmark bridge are calculated as follows:

1. Isolators placed at the top of the Cap beam
   - Post Yield *Stiffness* $K2{:}\ W/R = 2{,}432/5 = 486.4$ (KN/m)
   - Initial Stiffness $K1{:}\ 100 \times K2 = 100 \times 486.4 = 48{,}646$ (KN/m)
2. Isolators at top of Abutment
   - Post Yield Stiffness $K2{:}\ W/R = 6{,}632/5 = 1326.4$ (KN/m)
   - Initial Stiffness $K1{:}\ 100 \times K2 = 100 \times 1326.4 = 132{,}644$ (KN/m)

5.2 Impact damping modeling

The relations reflected at chapter 3 will be used in introducing a fictitious damper to be designed at modeling of the bridges to figure out the amount of energy dissipated during the rocking and pounding of the colliding bodies. To calculate the impact damping coefficients, we require to follow the below-mentioned steps:

Table 4. Steps of Damping Coefficients' Calculations

Step 1	ξ_{imp}	Damping ratio
Step 2	M_{eq}	Equivalent mass for deck-abutment and deck-cap beam interphases
Step 3	K_S	Impact stiffness for deck-abutment and deck-cap beam interphases
Step 4	$c_{imp} = 2\xi_{imp}\sqrt{K_S M_{eq}}$	Damping coefficients

- **Step 1: Damping Ratio**
  - The total dead load of the deck superstructure at the benchmark bridge is
  - W=$36,258$ KN
  - Considering the cross section of the girder, the distance to center of gravity is R = 4.24 m
  - Using the above-mentioned values, the mass moment of inertia is obtained as $I_0 = 85,094$
  - Using cross sectional dimensions of the deck, the degree of the slenderness of the rocking body (α) is calculated as 52.16°
  - By using the following formula, Coefficient of Restitution is calculated accordingly:

$$CR = \left(\frac{\dot{\theta}_2}{\dot{\theta}_1}\right)^2 = \left[1 - \frac{MR^2}{I_0}\left(1 - COS(2\alpha)\right)\right]^2$$

$$= [1 - \frac{36258 \times 4.24^2}{85,094}(1 - COS(104.32))]^2 = 0.164$$

– After calculating CR, damping ratio is calculated as:

$$\xi_{imp} = \frac{-\ln(CR)}{\sqrt{\pi^2 + (\ln(CR))^2}} = \frac{-\ln(0.164)}{\sqrt{\pi^2 + (\ln(0.164))^2}} = 0.498$$

Step 2: Equivalent mass for deck-abutment and deck-cap beam interphases

Table 5. Equivalent Mass Values

Weight of the Deck tributary area above Abutment (KN)	**Abutment Weight (KN)**	**Equivalent Mass (kg)**
4,864.62	50,000.00	452,070

Weight of the Deck tributary area above Pier (KN)	**Cap Beam Weight(KN)**	**Equivalent Mass (kg)**
13,264.42	2,585.00	220,605

- **Step 3: Impact stiffness for deck-abutment and deck-cap beam interphases**

For impact stiffness values at collision interphase, the stiffness of below motionless body is considered, in this respect:

Stiffness value for cap beam is calculated using cantilever beam stiffness formula and for abutment, stiffness it is assumed as 10 times the axial stiffness of bridge pier.

Table 6. Impact Stiffness Values

Stiffness of Abutment-Deck interphases (KN/m)	**Stiffness of Cap Beam-Deck interphases (KN/m)**
180,000,000.00	3,731,543.11

- **Step 4: Damping Coefficients**

After obtaining all the necessary values, using the $c_{imp} = 2\xi_{imp}\sqrt{K_S M_{eq}}$ formula, Impact damping coefficients are calculated for both cap beam-deck and abutment-deck interphases. The values are obtained as follows:

Table 7. Impact Damping Coefficients

Impact Damping Coefficient for Abutment-Deck interphases (KN*Sec/m)	**Impact Damping Coefficient for Cap Beam-Deck interphases (KN*Sec/m)**
290,778.39	28,629.70

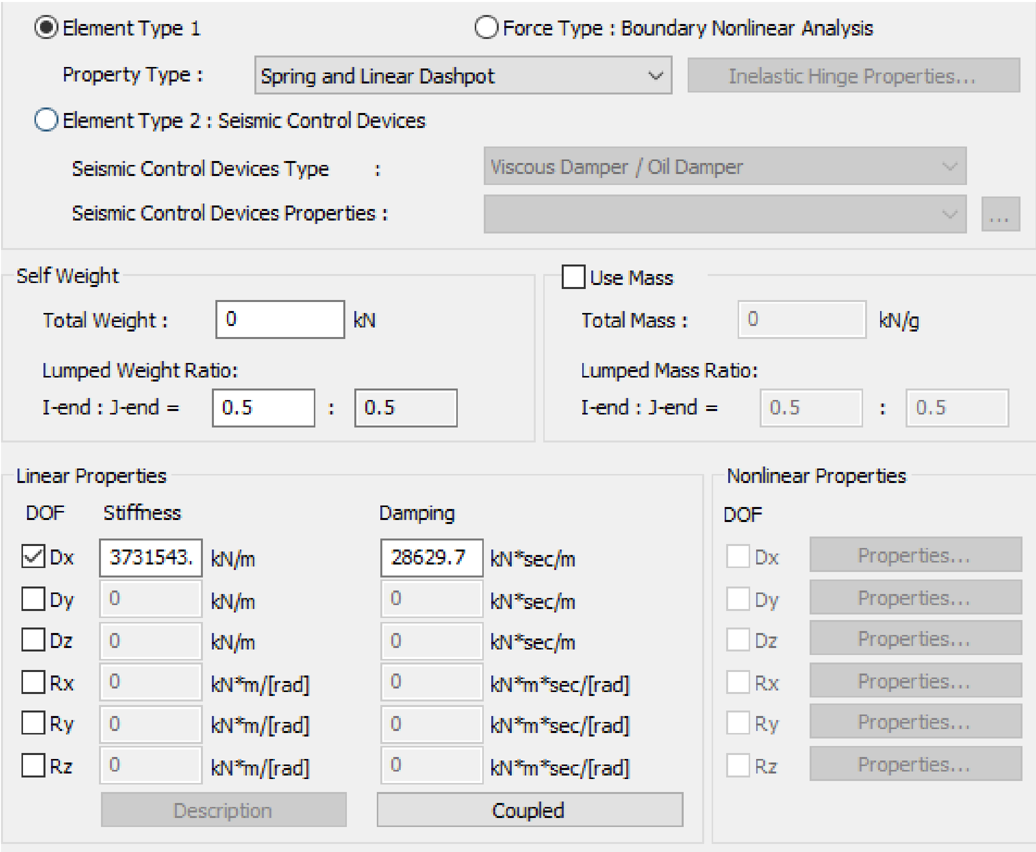

Figure 11. General Link Property Table Used to Define Spring and Dashpot Axial Properties

After obtaining all necessary values, the factious dampers are introduced to model being put just under the FPS isolators to account for energy dissipation as a result of the uplift and collision of the bodies.

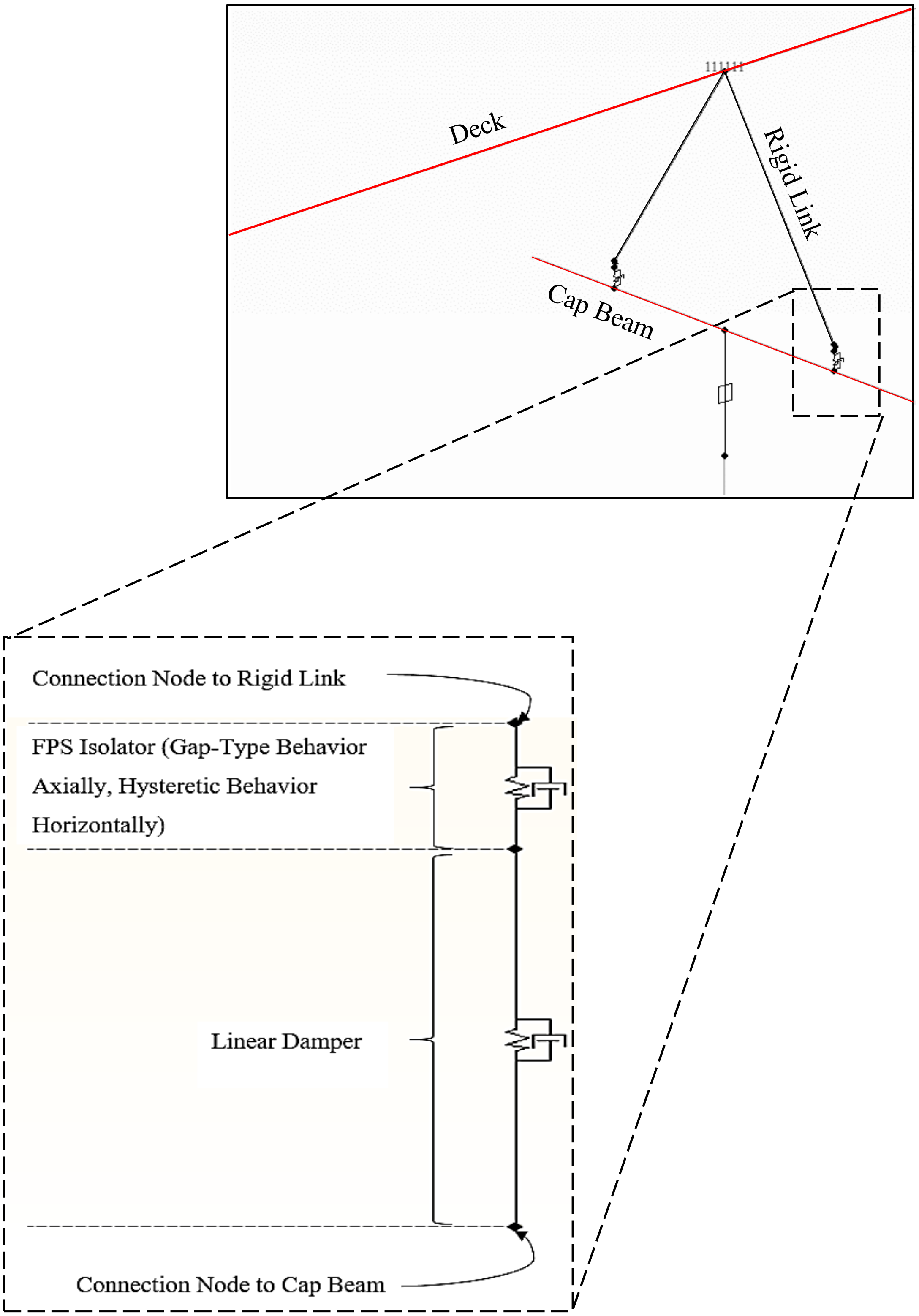

Figure 12. Connection Interphase of Linear Damper with FPS Isolator at MIDAS CIVIL

5.3 Modeling of Foundation, abutment and Related Soil–Structure Interaction

The type of bridges considered for this study have seat type abutment. For the modeling of the abutments, a separate model for abutments has been designed. and the equivalent nodal masses and springs reflecting the behavior and stiffness of the abutments and backfill have been added to main model. For the abutment model, a solid structure has been taken into account and the whole model together with wing walls are designed using thickness elements at Midas Civil. Foundation considered for model is namely rectangular shallow foundation for both the piers and abutments.

In order to take into account a behavior of the soil in which the foundation has been embedded into, guideline proposed at (Federal Emergency Management Agency, 2000) has been considered. The most important specification briefed about this approach is consideration of uncoupled spring model (3 Translational spring +3 Rotational) for reflection of the interaction between shallow bearing footings and their supporting soils. This approach has root in the works proposed by George Gazetas to be encountered in handling the stiffness solutions for any solid basement shape on the surface or partially or fully in a homogenous half-space (Gazetas, 1991).

Interaction between the abutment and backfill material and its simulation is an indispensable structural modeling aspect for engineers to be considered. Seat type abutments may experience a relatively larger seismic forces because of the effect of the dynamic backfill soil pressure and large inertial forces due to their massive sizes. To find out the stiffness of boundary springs in investigation and modeling of soil-abutment interaction, a relation associated with the ratio $\Delta/\mathbf{H}$ of abutment movement to abutment height is considered and in this respect a parameter called coefficient of subgrade reaction is developed by (G. W. Clough, J. M. Duncan, 1991) .

5.3.1 Foundation Design

Foundation considered for model is namely rectangular shallow foundation for piers. In order to design the foundation, the capacity design is made. In this step, the ultimate bearing capacity of the foundation is calculated.

Dimensions are as follows:

Table 8. Pier Footing Dimensions

Short Side (m)	20
Long Side (m)	30
Footing Thickness (m)	3.5
(Depth) (m)	6
Depth to Centroid of fo0ting (m)	4.25

Checking Ultimate Bearing Capacity: The considered footing dimensions are within the allowable range of bearing capacity, the corresponding in-detail calculations are as follows:

$$q_{ult}=cN_c F_{cs} F_{cd} F_{ci}+\gamma D_f N_q F_{qs} F_{qd} F_{qi}+0.5\gamma B N_\gamma F_{\gamma s} F_{\gamma d} F_{\gamma i}$$

Cohesive Intercept of sand equals zero, c = 0 →

$$q_{ult} = \gamma D_f N_q F_{qs} F_{qd} F_{qi} + 0.5\gamma B N_\gamma F_{\gamma s} F_{\gamma d} F_{\gamma i}$$

γ	Soil Unit Weight
D_f	Embedment Depth
	Bearing Capacity Factor for Soil Surcharge
N_q	Friction Angle $\emptyset = 40^0$
	$N_q = ((1+sin\emptyset1)/ (1-sin\emptyset1))* e\verb|^|\pi tan\emptyset$;
F_{qs}	Shape Factor $F_{qs} = (1+(B/L)\times sin\emptyset)$
	Depth Factor
F_{qd}	If $\frac{D}{B} \leq 1 \rightarrow \; F_{qd} = 1 + 2\tan\emptyset(1-\sin\emptyset)^2(\frac{\mathrm{D}}{\mathrm{B}})$
	If $\frac{D}{B} > 1 \rightarrow \; F_{qd} = 1 + 2\tan\emptyset(1-\sin\emptyset)^2\tan^{-1}(\frac{\mathrm{D}}{\mathrm{B}})$
F_{qi}	F_{qi}=[1−$arctan(Qtr/Qaxisl)$/ 90^0]^2
N_γ	N_γ=1.5(Nq−1) $tan\emptyset$
$F_{\gamma s}$	$F_{\gamma s}$=1−0.4(B/L)
$F_{\gamma d}$	$F_{\gamma d}$=1
$F_{\gamma i}$	$F_{\gamma i}$=[1−$arctan(Qtr/Qaxisl)$/ φ]

Table 9. Ultimate Bearing Capacity Parameters

		$N_{\gamma/q}$	$F_{\gamma s/qs}$	$F_{\gamma d/qd}$	$F_{\gamma i/qi}$
Short Side	γ	79.540	0.867	1	0.182
	q	64.195	1.213	1.128	0.555
Long Side	γ	79.540	0.673	1	0.134
	q	64.195	1.524	1.078	0.516

Gazetas Springs: To account for the interaction among soil and footing, Gazetas Springs are considered for which the corresponding in-detail calculations are as follows;

Table 10. Ground Soil Properties

V	Poisson Ratio	0.35
γ	Unit Weight of Soil	20 KN/m^3
$\boldsymbol{\nu_s}$	Shear Wave Velocity	563.88 m/s
$G_{zero} = (\gamma \times \boldsymbol{\nu_s}^2)/\boldsymbol{g}$	Initial Shear Modulus	648237.83 KN/m^2
G	Shear Modulus	413251.61 KN/m^2
$R_f = G/G_0$	Effective Shear Modulus Ratio	0.64

$$k_{x,sur} = \frac{GB}{2-v}\left[3.4\,(\frac{L}{B})^{0.65} + 1.2\right] \quad \text{Translation along x-axis} \quad (10)$$

$$k_{y,sur} = \frac{GB}{2-v}\left[3.4\,(\frac{L}{B})^{0.65} + 0.4\,\frac{L}{B} + 0.8\right] \quad \text{Translation along y-axis} \quad (11)$$

$$k_{z,sur} = \frac{GB}{1-v}\left[1.55\,(\frac{L}{B})^{0.75} + 0.8\right] \quad \text{Translation along z-axis} \quad (12)$$

$$k_{xx,sur} = \frac{GB^3}{1-v}\left[0.4\,(\frac{L}{B})^{0.65} + 0.1\right] \quad \text{Rocking about x-axis} \quad (13)$$

$$k_{yy,sur} = \frac{GB^3}{1-v}\left[0.47\,(\frac{L}{B})^{2.4} + 0.034\right] \quad \text{Rocking about y-axis} \quad (14)$$

$$k_{zz,sur} = GB^3\left[0.53\,(\frac{L}{B})^{2.45} + 0.51\right] \quad \text{Torsion about z-axis} \quad (15)$$

Figure 13. Footing with specified dimensions at Surface

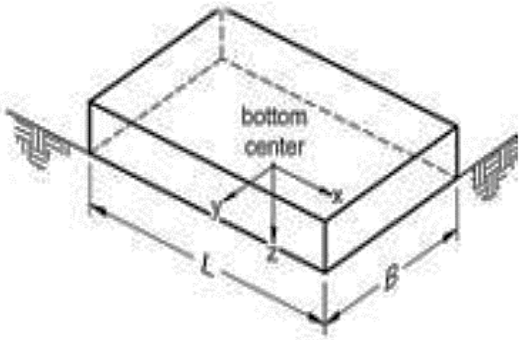

$$\beta_x = (1+ 0.21\sqrt{\frac{D}{B}}).\left[1 + 1.6\left(\frac{hd(B+L)}{BL^2}\right)^{0.4}\right] \tag{16}$$

Translation along x-axis

$$\beta_y = \beta_x \tag{17}$$

Translation along y-axis

$$\beta_z = \left[1 + \frac{1}{21}\frac{D}{B}\left(2 + 2.6\,\frac{B}{L}\right)\right].\left[1 + 0.32\left(\frac{d(B+L)}{BL}\right)^{2/3}\right] \tag{18}$$

Translation along Z-axis

$$\beta_{XX} = 1 + 2.5\frac{d}{B}\left[1 + \frac{2d}{B}\left(\frac{d}{D}\right)^{-0.2}\sqrt{\frac{B}{l}}\right] \tag{19}$$

Rocking about x-axis

$$\beta_{yy} = 1 + 1.4\left(\frac{d}{L}\right)^{0.6}\left[1.5 + 3.7\left(\frac{d}{L}\right)^{1.9}\left(\frac{d}{D}\right)^{-0.6}\right] \tag{20}$$

Rocking about y-axis

$$\beta_{ZZ} = 1 + 2.6\left(1 + \frac{B}{L}\right)\left(\frac{d}{B}\right)^{0.9} \tag{21}$$

Torsion about z-axis

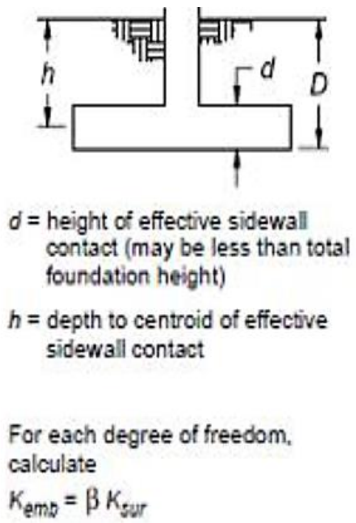

Figure 14. Footing with specified Dimensions at Embedment Depth

Using the equations 10 to 21, the required spring stiffness values are calculated and entered at benchmark bridge model to resemble the soil-footing interaction. At following tables, the calculated values are tabulated accordingly:

Table 11. Stiffness of Foundation at Surface

Kx,sur	28177520	kN/m
Ky,sur	29179342.53	kN/m
Kz,sur	36885881	kN/m
Kxx,sur	12016085422	kN.m/rad
Kyy,sur	6498622306	kN.m/rad
Kzz,sur	6417622767	kN.m/rad

Table 12. Correction Factors for Embedment

Bx	1.613751293
By	1.613751293
Bz	1.201576155
Bxx	1.576757025
Byy	1.6118891
Bzz	1.902726811

Table 13. Stiffness of Foundation Adjusted to Depth of Embedment

Kx,emb	45471510	kN/m
Ky,emb	47088202	kN/m
Kz,emb	44321195	kN/m
Kxx,emb	18946447104	kN.m/rad
Kyy,emb	10475058462	kN.m/rad
Kzz,emb	12210982904	kN.m/rad

5.3.2 Abutment Design

The stiffness value for each layer of elevation can be found by multiplying the coefficient of horizontal subgrade reaction by related node's territory area. In addition to the springs in reflecting the backfill soil pressure, another set of translational springs are also encountered in design of the model to reflect shear strength of the backfill. In doing this it has been assumed that the portion showing shear strength is only that portion between the wing walls will deform in shearing mode as bridge moves in the transverse direction (Murat Dicleli, Jung -Yoon LEE and Mohamad Mansour, 2004)

- Backfill pressure

$\boldsymbol{k_{sh}} = (\frac{\mathbf{14500}}{\boldsymbol{H}}) \times \mathrm{z}$ Coefficient of Subgrade Reaction

Table 14. Compression-Only Stiffness Values for each Layer of Abutment (Back-wall + Wing-walls)

Elevation Z	For external nodes of thickness element	For middle nodes of thickness element
1	1318.181818	659.0909091
2	2636.363636	1318.181818
3	3954.545455	1977.272727
4	5272.727273	2636.363636
5	6590.909091	3295.454545
6	7909.090909	3954.545455
7	9227.272727	4613.636364
8	10545.45455	5272.727273
9	11863.63636	5931.818182
10	13181.81818	6590.909091
11	14500	7250

- Shear stifness at the Portion Between Wing-Walls

$$k_{sh} = \frac{G.B.H}{l}$$

By considering the above-mentioned formula, shear strength value for the portion between Wing-Walls can be calculated and Equally distributed to interphase nodes between Abutment-Backfill.

Table 15. Abutment Dimensions

Abutment Height (m)	11
Abutment Width (m)	18
Seat Wall Thickness(m)	2
Wing Wall thickness (m)	0.5
Wing Wall length (m)	6

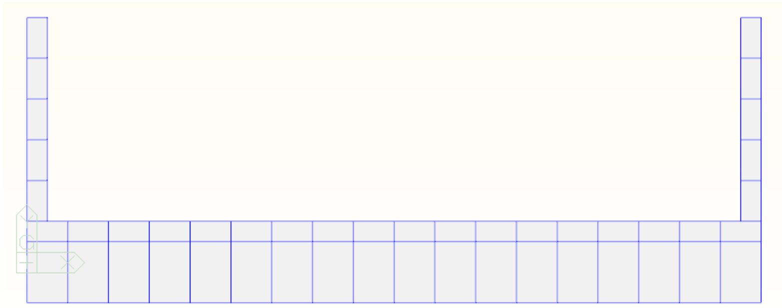

Figure 15.Top View of The Abutment Backwall and Wingwalls

Following application of all these boundary springs as well as Gazetas springs of abutment footing, at the final stage, in order to reflect the behavior of abutment at benchmark bridge model, another simple model containing only nodal mass and connecting link with equivalent stiffness to stiffness of abutment model is taken into account. In an iterative manner, through assigning a various nodal mass values to this new model, the deformation amounts observed are compared with abutment model's deformation in order to find the most optimum nodal mass value which as a result of loading in horizontal directions leads to same horizontal deformation of abutment model. At the end of several trials, nodal mass values in X and Y directions together with associated force deformation relationships obtained, are entered to Benchmark bridge's model through application of Point Springs.

Figure 16. Abutment Model Designed Using Thickness Elements at MIDAS Civil.

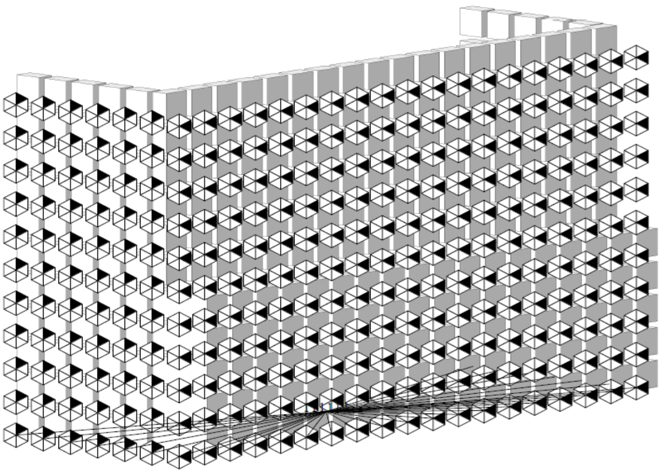

CHAPTER 6

DESIGN SPECTRA AND SELECTED GROUND MOTIONS

For the aim of this study, seven earthquake ground motions whose response spectra are compatible with the AASHTO spectrum for soil type C (soft clay) are chosen. The resource used to acquire motion sets belongs to university of California, Berkley namely PEER (Pacific Earthquake Engineering Research) ground motion database. The ground type criteria selected for the aim of analysis is type C (soft clay and sand) and the reason for this is the geological composition of the Çanakkale region of Turkey. The design peak ground acceleration for the site is 0.7 g and AASHTO spectrum is framed based on this value. The ground motions obtained for this study are scaled for the period range of 0.5T and 1.25T as presented in the Fig 17. Unlike the conventional bridge design for which the scaling range being considered is usually 0.2T and 1.5 T , for the seismically isolated structures codes provide narrower range (Naeim, 2004). Details of the selected ground motions are provided at table 16. Scaling method used in the study is minimum mean square error (MSE) scaling method for which , 14 points are chosen in the aforementioned period range between 1.86 and 4.46. In MSE scaling method, a quantitative measure of the overall fit of the record to a target spectrum is the mean squared error (MSE) between the target spectrum and the response spectrum of a recorded time history. For this purpose the period range of interest (0.5 T to 1.25T) is subdivided into a large number of points equally-spaced and the target and record response spectra are interpolated to provide spectral acceleration at each period, respectively (Elnaz Amirzehni, 2015)

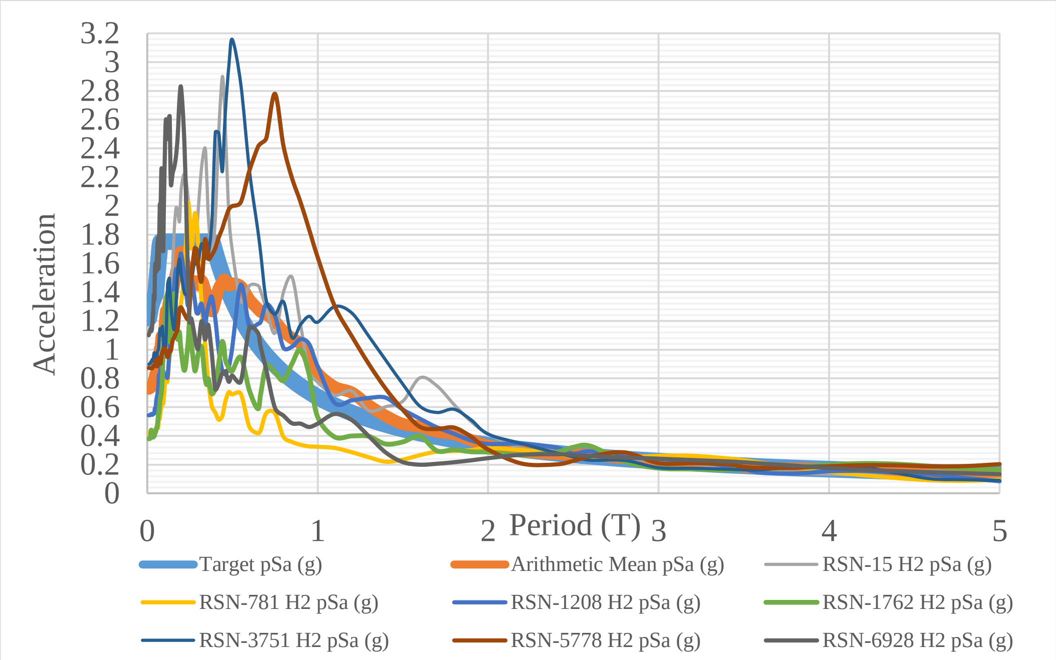

Figure. 17 Target Design Spectrum and Average of Response Spectra of Selected Ground Motions

Table 16. Details and Properties of the Selected Ground Motions

Earthquake Name	Year	Magnitude	Station Name	Vs30 (m/sec)	Scale Factor
"Kern County"	1952	7.36	"Taft Lincoln School"	385.43	4.85
"Loma Prieta"	1989	6.93	"Lower Crystal Springs Dam dwnst"	586.08	4.7
"Chi-Chi_ Taiwan"	1999	7.62	"CHY046"	442.15	2.85
"Hector Mine"	1999	7.13	"Amboy"	382.93	2.51
"Cape Mendocino"	1992	7.01	"South Bay Union School"	459.04	4.4
"Iwate_ Japan"	2008	6.9	"Matsuyama City"	436.34	2.94
"Darfield_New Zealand"	2010	7	"LPCC"	649.67	3.0

CHAPTER 7

DISCUSSION OF PARAMETRIC NONLINEAR TIME-HISTORY ANALYSES RESULTS

The structural models of the Uplift-Allowed and Uplift-Restricted bridges are designed and Non Linear Time History Analysis (NTHA) of the bridge models has been carried out being subject to seven ground motions chosen for this research study. The NLTHA are repeated for different peak ground acceleration values for each selected earthquake ground motion. This resulted in 117 different analysis cases in total. All the analyses results comparing the difference in performances and responses of Uplift-Allowed and Uplift-Restricted Models are reflected at following subsections considering the average of the results from the seven ground motions for different values of peak ground acceleration in terms of pier moment response, pier base shear response and bearings' axial loads.

7.1 Comparison of Uplift-Allowed and Uplift-Restricted Bridge Models in Terms of Span Number factor

The figures clearly demonstrate the improved seismic behavior of bridge at higher span number values as a result of associated superstructure rocking action. The results of the various analysis and comparisons done among 2 different cases of Uplift –Allowed and Uplift-Restricted models reveal the fact that the rocking action decreases the seismic action response on bridge pier considerably in terms of moment response and base shear. Moreover, the accuracy of the fact can also be confirmed by looking at the trend established among behavior of models under different ground motion intensities. The significant response difference at higher span numbers under severe ground motions is clear evidence of this claim. Besides, another important point to be noted down regarding the effect of span number on behavior of bridges at both Uplift-Allowed and Uplift-Restricted cases is related to torsional rigidity of the structure which can be understood by looking deeply to trend of the graphics under transverse motion only from 4 span number model onwards, as indicated previously, the effect of the rocking action still shows its impact but the ratio of response at 5 span and 6 span bridge models is not as high as 4 span. Models with higher Span number have lower torsional rigidity which causes the structure to not to have expected uplift at all connection phases which eventually decreases the efficiency of the action to some limited degree at some cases.

7.1.1 Effect of Span Number Factor Investigated Under the Effect of Transverse Motion

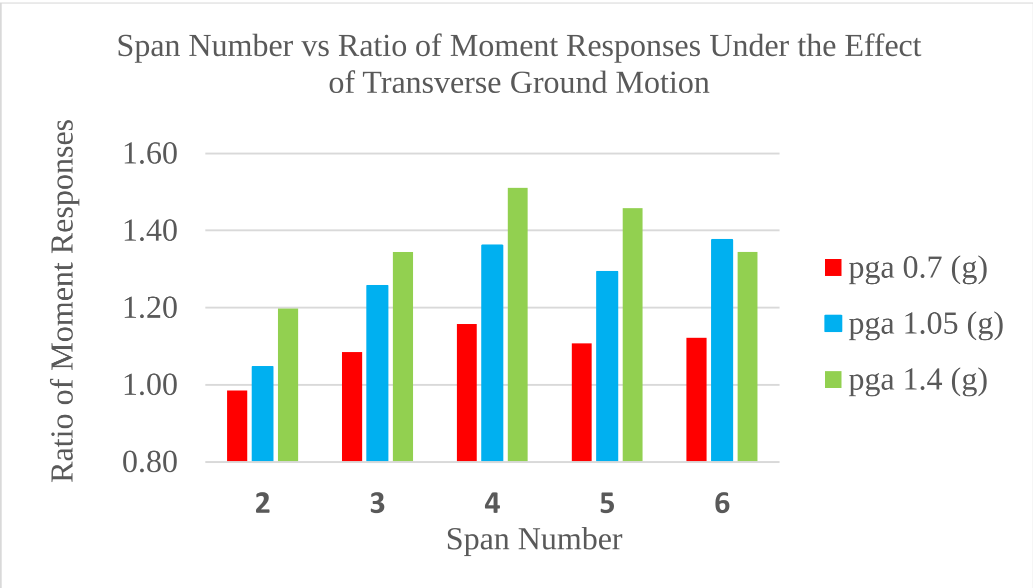

Figure 18. Span Number and Ratio of Moment Responses of Uplift-Restricted Case to Uplift-Allowed Case (Investigated Under the Effect of Transverse Motion Considering Three different PGA values)

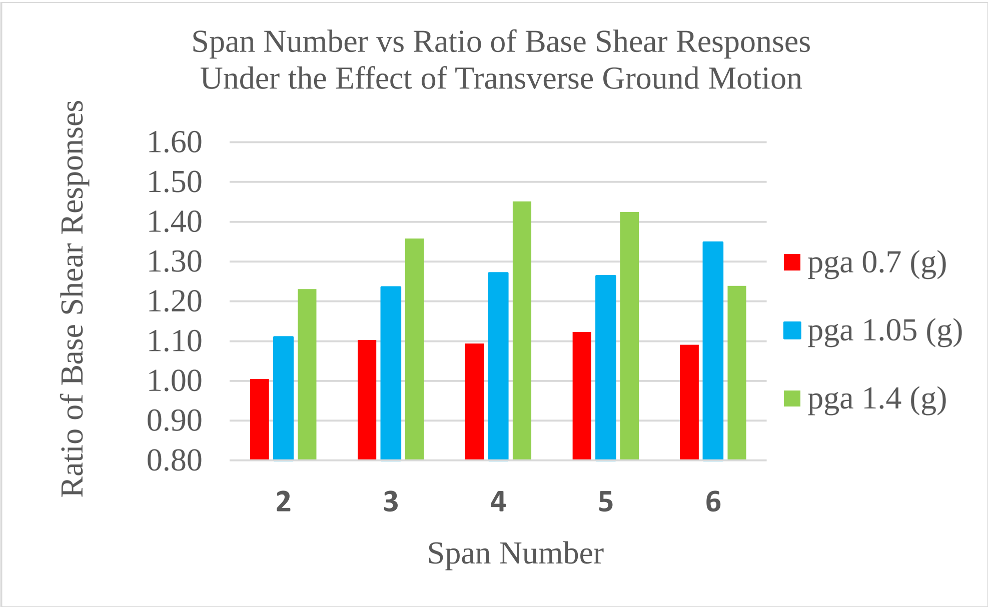

Figure 19. Span Number and Ratio of Base Shear Responses of Uplift-Restricted Case to Uplift-Allowed Case (Investigated Under the Effect of Transverse Motion Considering Three different PGA values)

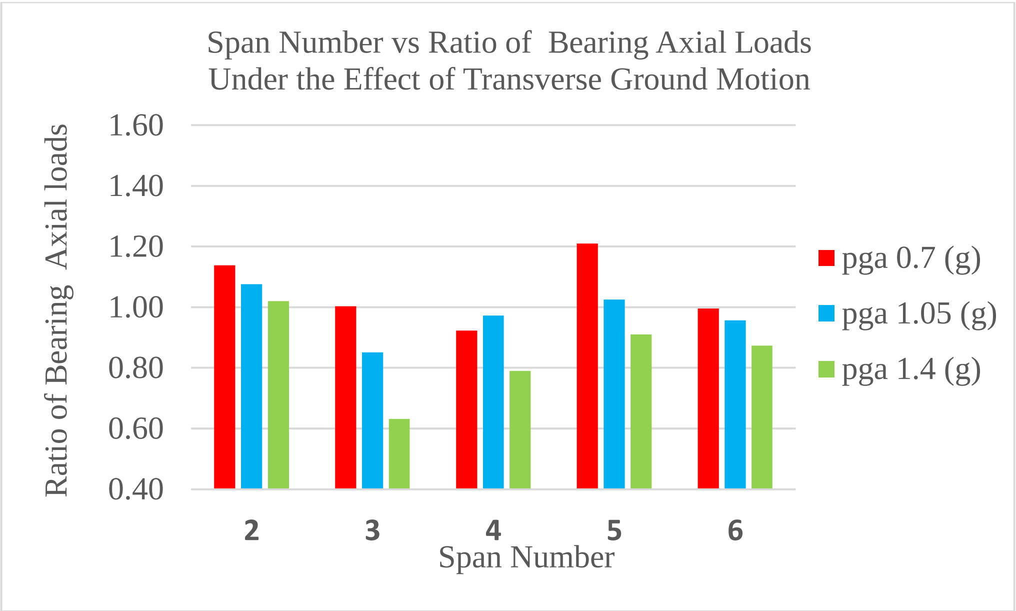

Figure 20. Span Number and Ratio of Bearing Axial Loads of Uplift-Restricted Case to Uplift-Allowed Case (Investigated Under the Effect of Transverse Motion Considering Three different PGA values)

7.1.2 Effect of Span Number Factor Investigated Under the Combined Effect of Transverse and Vertical Motions

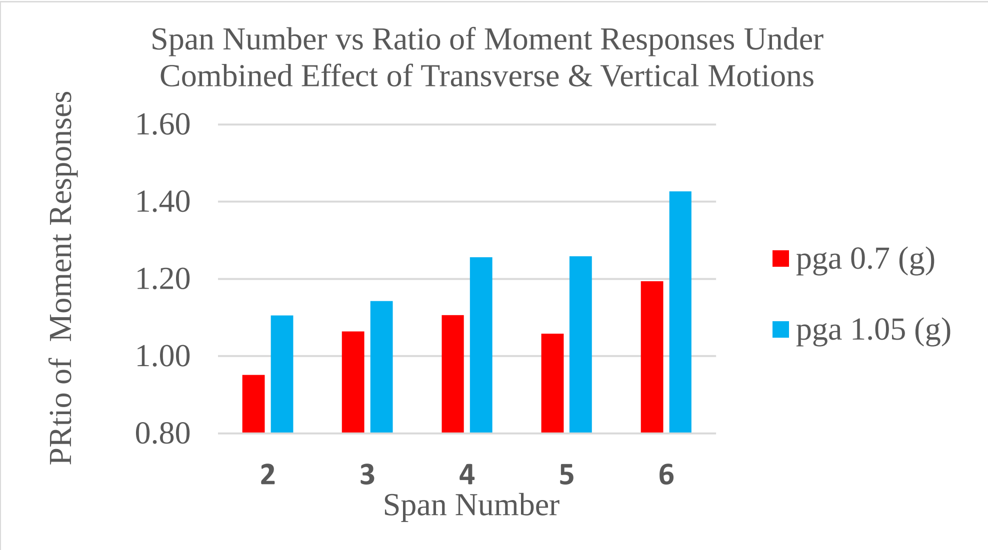

Figure 21. Span Number and Ratio of Moment Responses of Uplift-Restricted Case to Uplift-Allowed Case (Investigated Under the Combined Effect of Transverse and Vertical Motions Considering Two different PGA values)

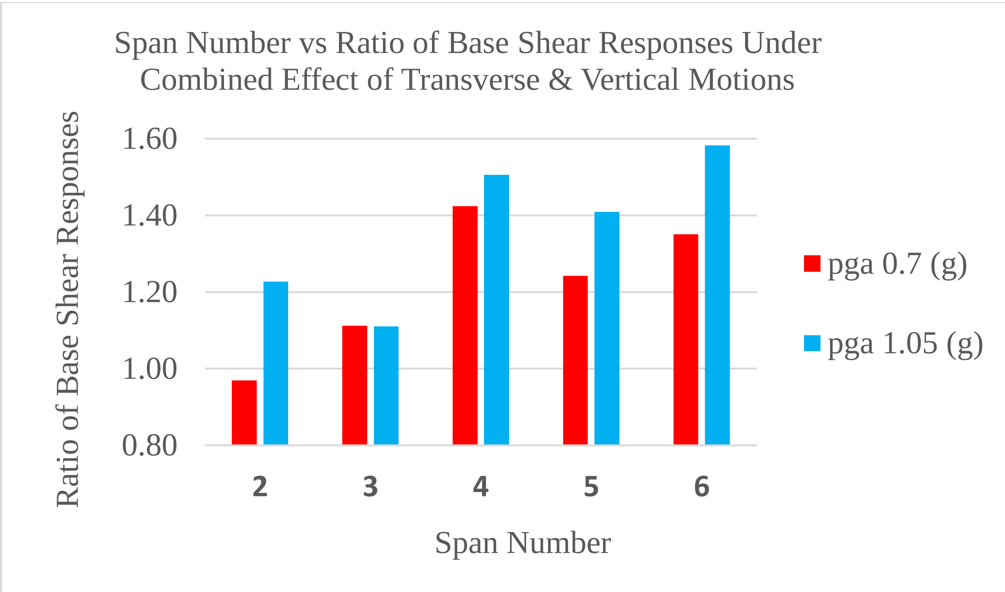

Figure 22. Span Number and Ratio of Base Shear Responses of Uplift-Restricted Case to Uplift-Allowed Case (Investigated Under the Combined Effect of Transverse and Vertical Motions Considering Two different PGA values)

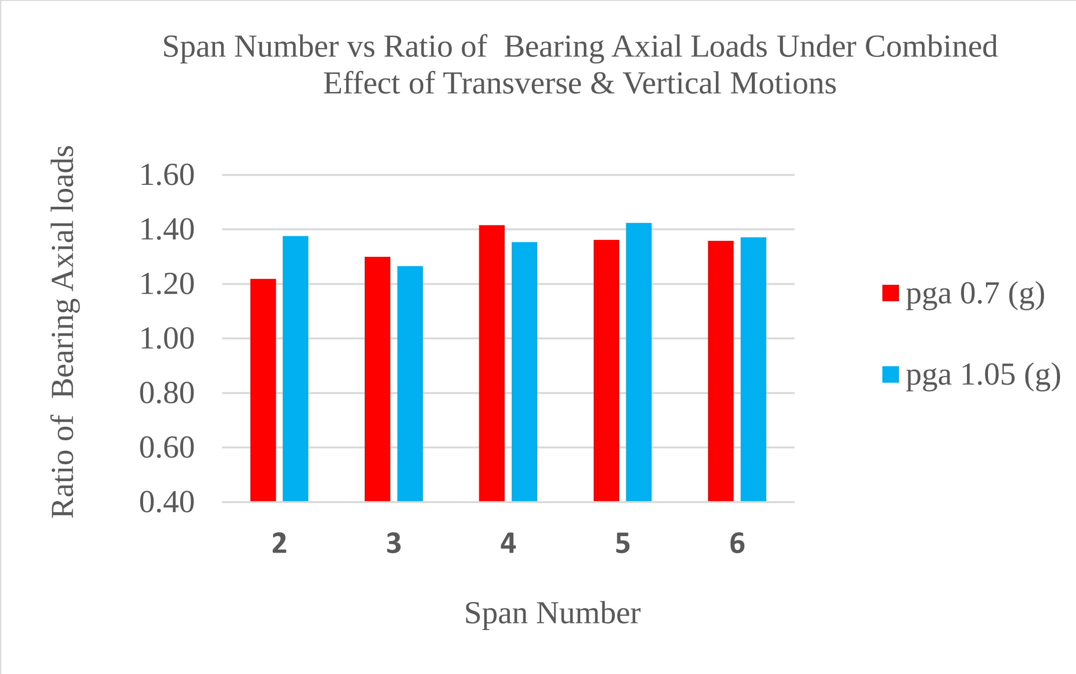

Figure 23. Span Number and Ratio of Bearing Axial Load of Uplift-Restricted Case to Uplift-Allowed Case (Investigated Under the Combined Effect of Transverse and Vertical Motions Considering Two different PGA values)

7.2 Comparison of Uplift-Allowed and Uplift-Restricted Bridge Models in Terms of FPS Bearing Line Distances

In this part, performance of the Uplift-Allowed bridges and Uplift-Restricted bridges is compared in terms of the distance between their bearings. The analyses results reflected that the pier moment and base shear responses of Uplift-Restricted bridges are larger than those of Uplift-Allowed ones regardless of the distance between bearings. However, the difference between the pier responses of Uplift-Allowed and Uplift-Restricted bridges becomes more pronounced as the bearing line distance to the pier axis gets smaller. The main reason for this is that, the susceptibility of superstructure deck to undergo rocking decreases as the bearing line distance to pier axis increases. The logic established can be better understood if the bearing line distance to pier axis be considered as moment arm. This eventually leads Uplift-

Allowed models to behave similar to Uplift-Restricted bridges without having a major uplift during a seismic excitation.

7.2.1 Effect of Bearing Distances Investigated Under the Effect of Transverse Motion

Figures 24 and 25 clearly demonstrate the results of this research study where the ratios of Uplift-Restricted to Uplift-Allowed pier responses are illustrated with respect to different bearing line distance values to pier axis. The response ratios presented for both figures are all larger than 1. This clearly shows the improved seismic behavior of Uplift-Allowed bridges with respect to Uplift-Restricted ones. At the same time at both figures, the ratio of Uplift-Restricted to Uplift-Allowed responses shows a decreasing trend as the rocking amount of superstructure deck decreases. In relation with these observations, the results of the analyses for this case also show an increasing trend at ratio of bearing axial load ratio of Uplift-Restricted bridges to Uplift-Allowed ones which is also another clear evidence of observed behavior; as the value of bearing line distance to pier axis decreases, the rocking phenomenon occurring probability increases at superstructure deck and this leads to more axial load being transferred to each corner of rocking block; in this case, each FPS sliding bearing.

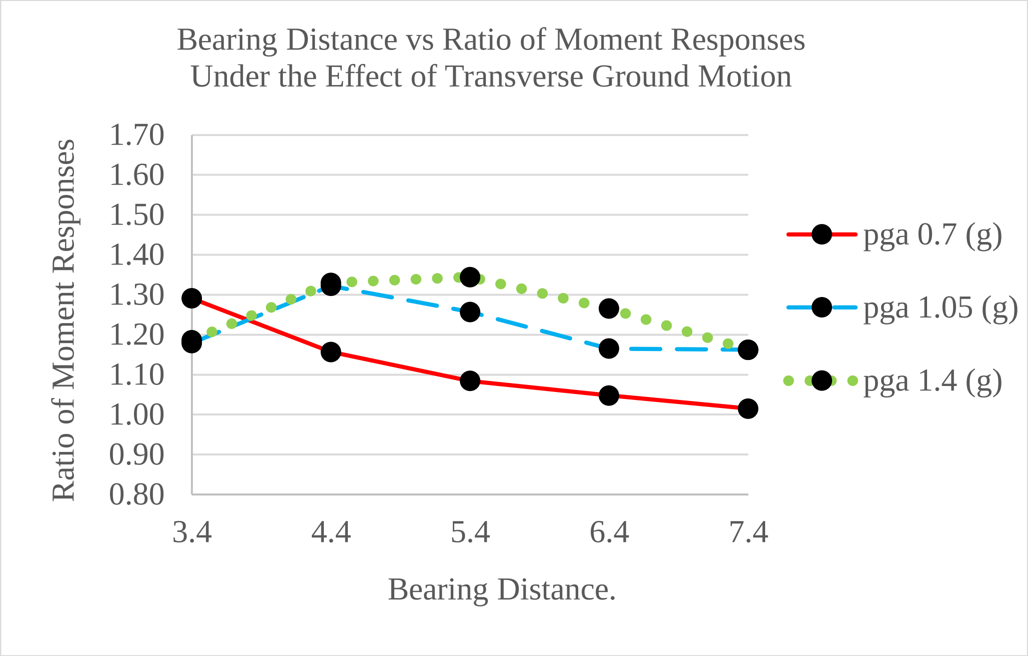

Figure 24. Bearing Distances and Ratio of Moment Responses of Uplift-Restricted Case to Uplift-Allowed Case. (Investigated Under the Effect of Transverse Motion Considering Three Different PGA values)

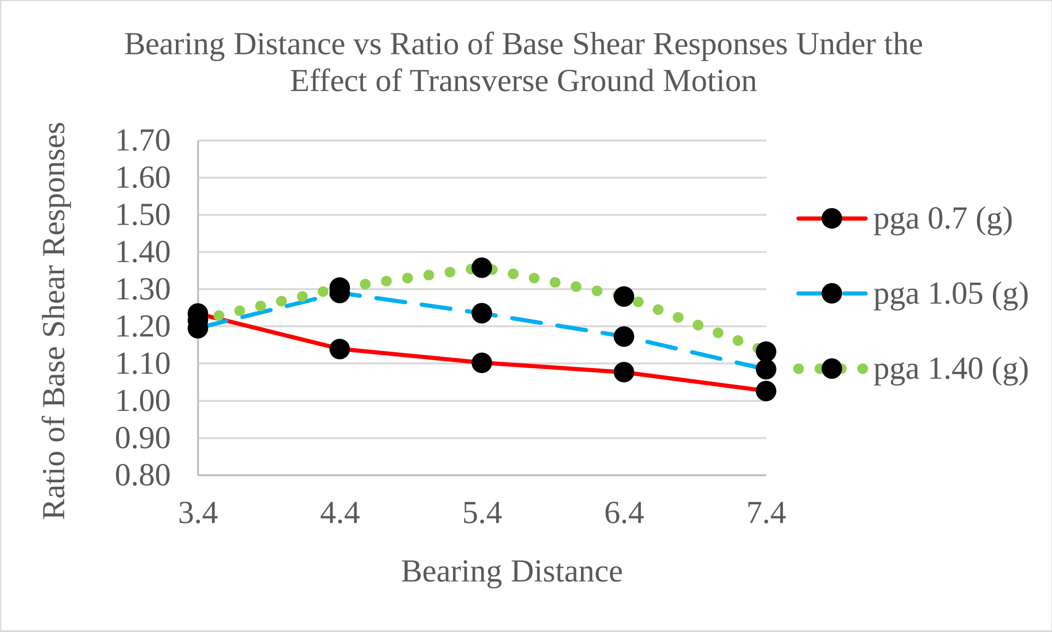

Figure 25. Bearing Distances and Ratio of Base Shear Responses of Uplift-Restricted Case to Uplift-Allowed Case (Investigated Under the Effect of Transverse Motion Considering Three Different PGA values)

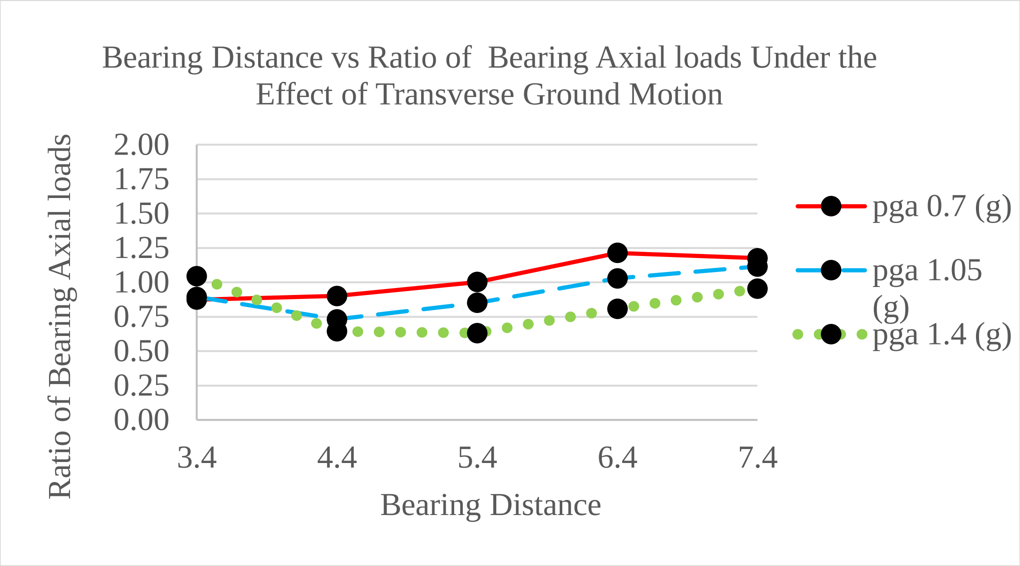

Figure 26.Bearing Distances and Ratio of Bearing Axial Loads of Uplift-Restricted Case to Uplift-Allowed Case (Investigated under the Effect of Transverse Motion Considering Three Different PGA values)

7.2.2 Effect of Bearing Distances Investigated Under the Combined Effect of Transverse and Vertical Motions

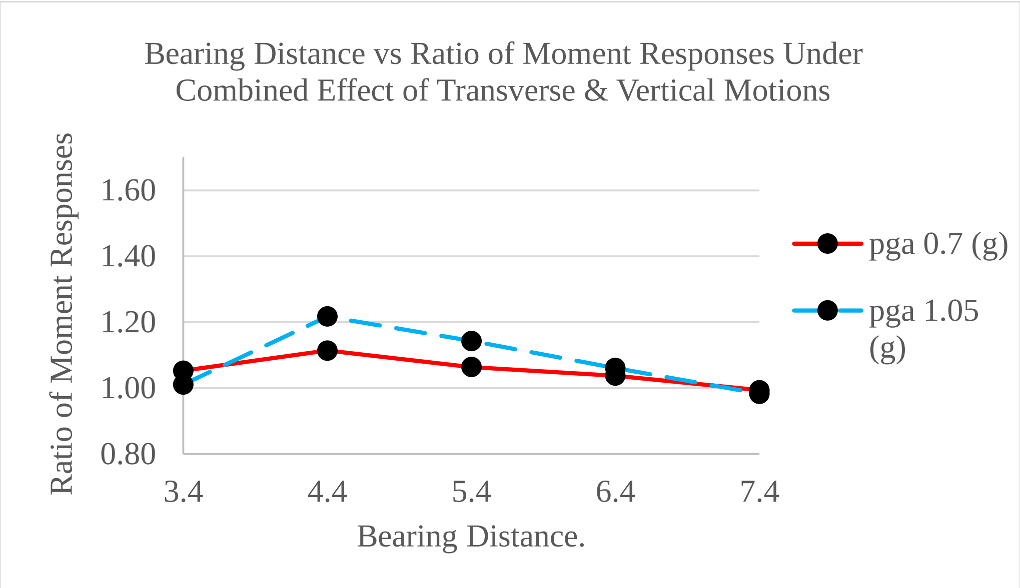

Figure 27. Bearing Distances and Ratio of Moment Responses of Uplift-Restricted Case to Uplift-Allowed Case (Investigated Under the Combined Effect of Transverse and Vertical Motions Considering Two Different PGA values)

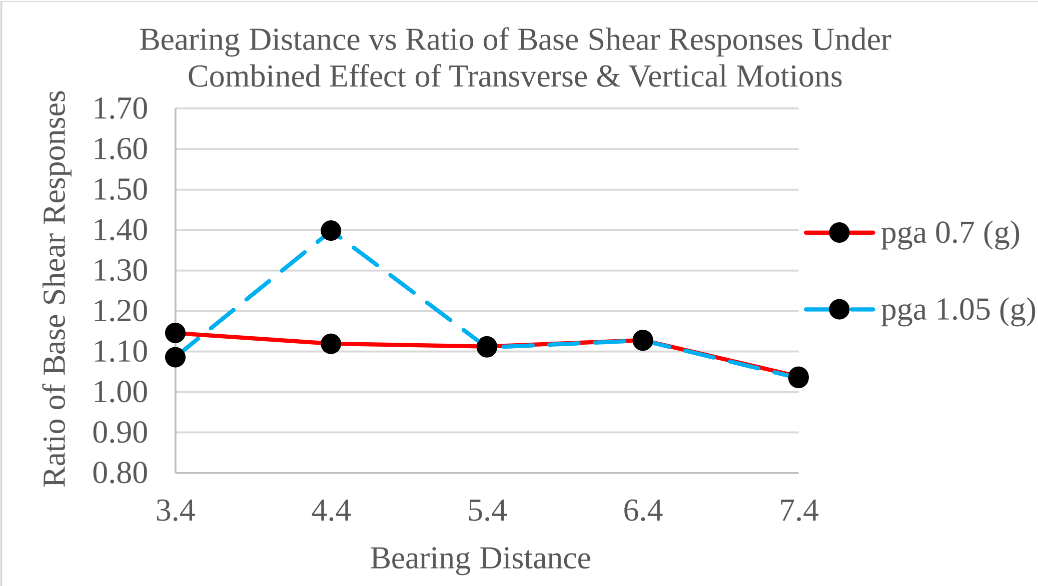

Figure 28. Bearing Distances and Ratio of Base Shear Responses of Uplift-Restricted Case to Uplift-Allowed Case (Investigated Under the Combined Effect of Transverse and Vertical Motions Considering Two Different PGA values)

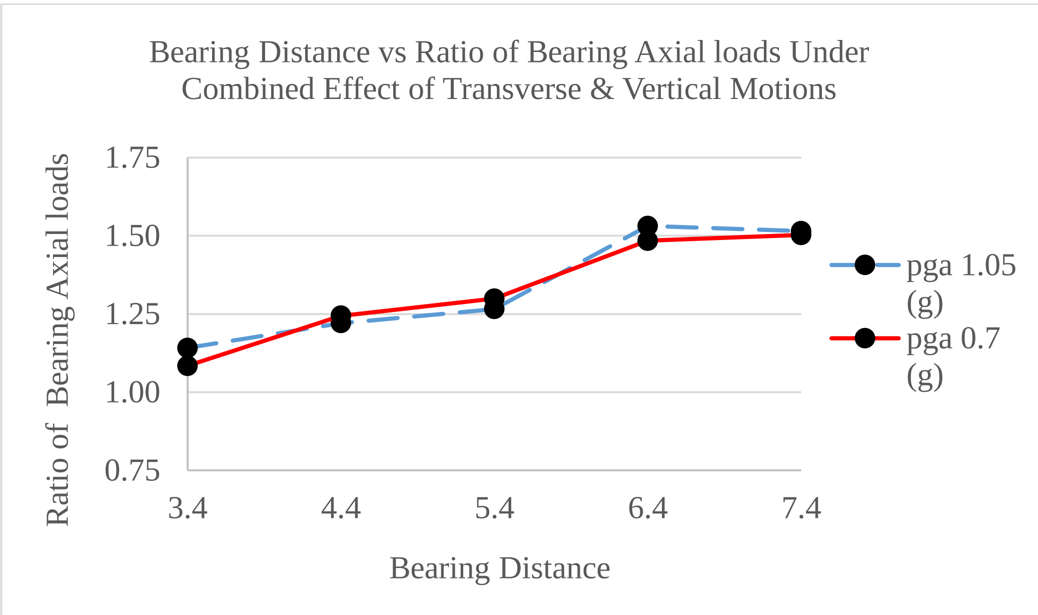

Figure 29. Bearing Distances and Ratio of Bearing Axial Load of Uplift-Restricted Case to Uplift-Allowed Case (Investigated Under the Combined Effect of Transverse and Vertical Motions Considering Two Different PGA values)

7.3 Comparison of Uplift-Allowed and Uplift-Restricted Bridge Models in Terms of Span Length factor

In this part, a comparative assessment of Uplift-Allowed bridges with Uplift-Restricted bridges is discussed with respect to span length factor. The analyses reflected that the pier moment and base shear responses of Uplift-Restricted bridges are larger than those of Uplift-Allowed ones regardless of the span length of the bridges. Results of the analyses carried out under only transverse motion with different ground motion intensity values for bridge models with various span length dimensions ranging between 30 and 70 meters show that for each pair of Uplift-Allowed and Uplift-Restricted models under PGA 0.7 and 1.05, the trend is somehow stable and the ratio of the responses of Uplift- Restricted to Uplift-Allowed bridge models do not show that much change with respect to span length factor, (ratio for PGA 0.7 is 1.10 and for PGA 1.05 is around 1.2). However, the trends observed at figures 30 and 31 show that for the pair of bridge models analyzed under PGA 1.4, this ratio of Uplift-Restricted bridge responses to Uplift-Allowed ones gets relatively an increasing trend in relation with increase in span length. By looking at to figure 30, it can be observed that, the ratio of moment response for 70 meters span length is considerably high around 1.4 which is an indication of improved seismic performance of Uplift-Allowed bridges with higher span length value under severe ground motions. The reason for this is that, the bridge models with longer span lengths are weightier than the other ones and this factor inherently affects the amount of energy being damped out during collision of superstructure deck with substructure as a result of rocking action. The results of the analysis under combined transverse and vertical motion also supports the idea of improved seismic response for Uplift-Allowed bridges.

7.3.1 Effect of Span Length Factor Investigated Under the Effect of Transverse Motion

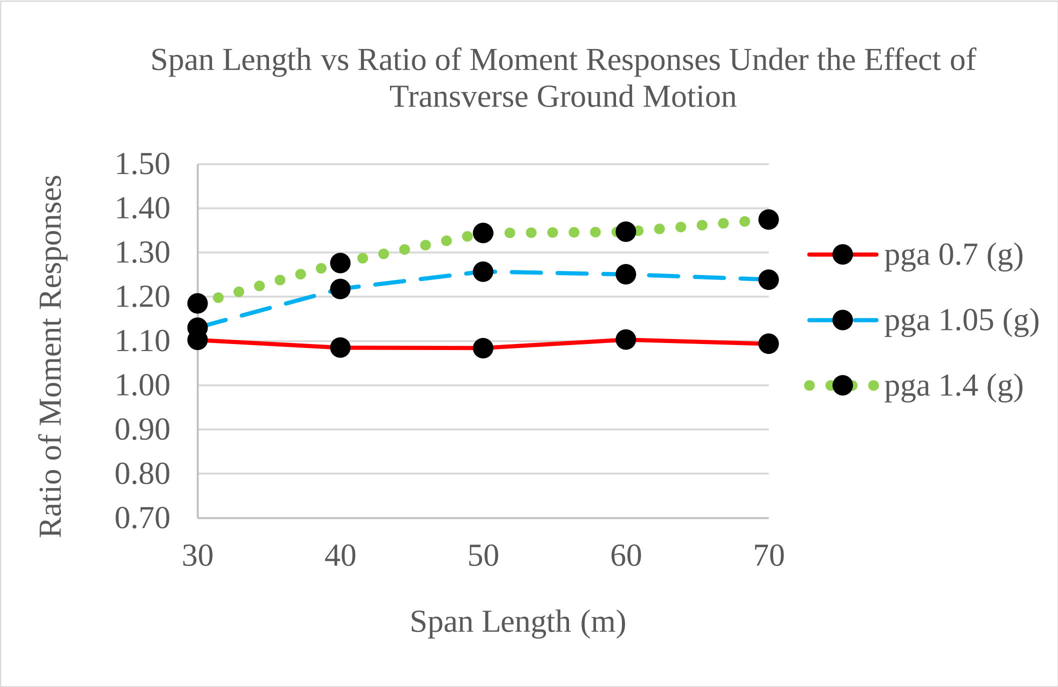

Figure 30. Span Length and Ratio of Moment Responses of Uplift-Restricted Case to Uplift-Allowed Case (Investigated Under the Effect of Transverse Motion Considering Three Different PGA values)

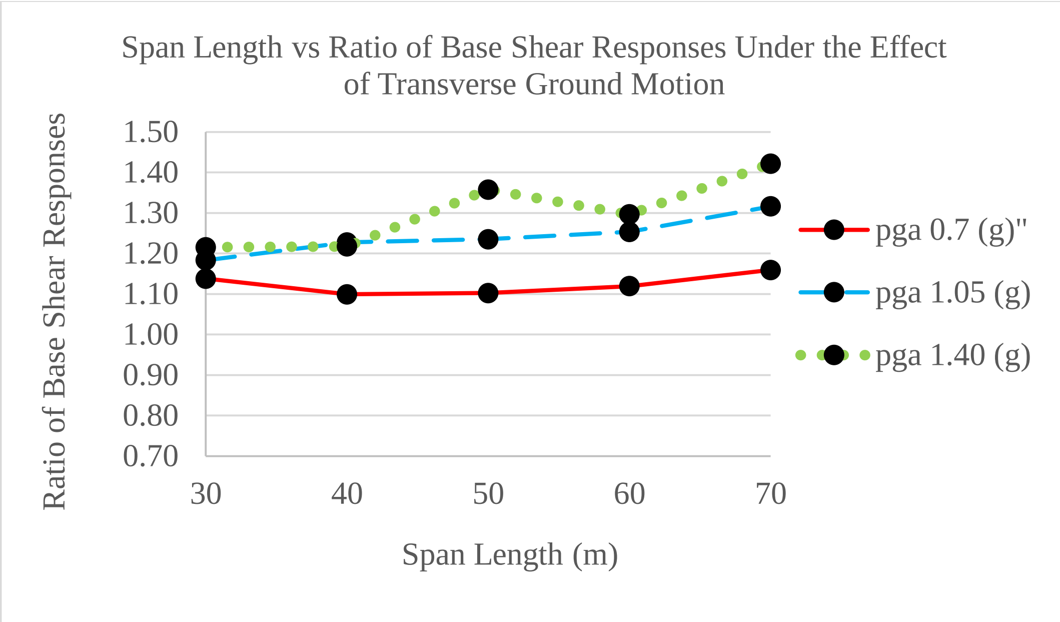

Figure 31. Span Length and Ratio of Base Shear Responses of Uplift-Restricted Case to Uplift-Allowed Case (Investigated Under the Effect of Transverse Motion Considering Three Different PGA values)

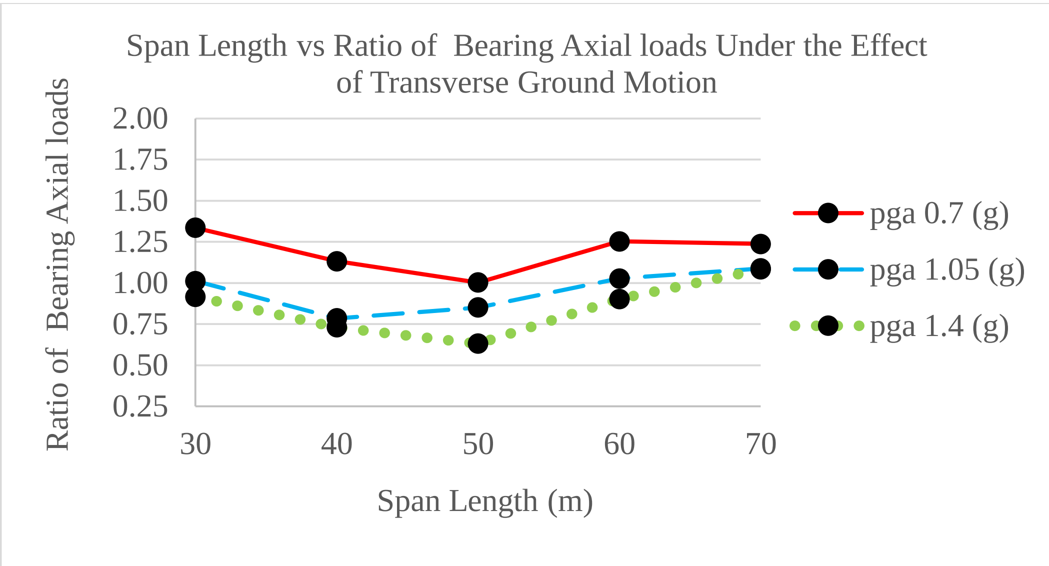

Figure 32. Span Length and Ratio of Bearing Axial Loads of Uplift-Restricted Case to Uplift-Allowed Case (Investigated Under the Effect of Transverse Motion Considering Three Different PGA values)

7.3.2 Effect of Span Length Factor Investigated Under the Combined Effect of Transverse and Vertical Motions

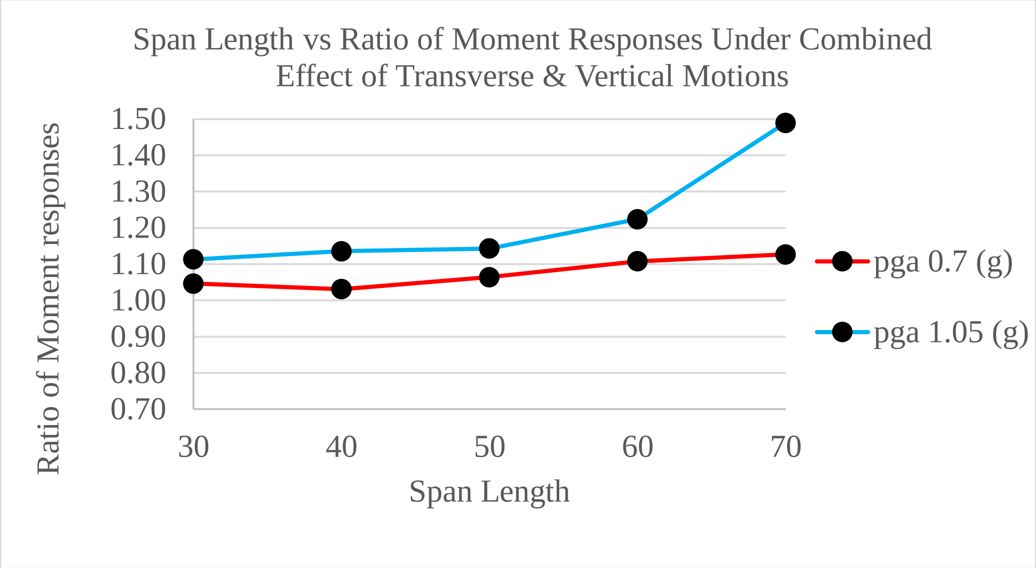

Figure 33. Span Length and Ratio of Moment Responses of Uplift-Restricted Case to Uplift-Allowed Case (Investigated Under the Combined Effect of Transverse and Vertical Motions Considering Two Different PGA values)

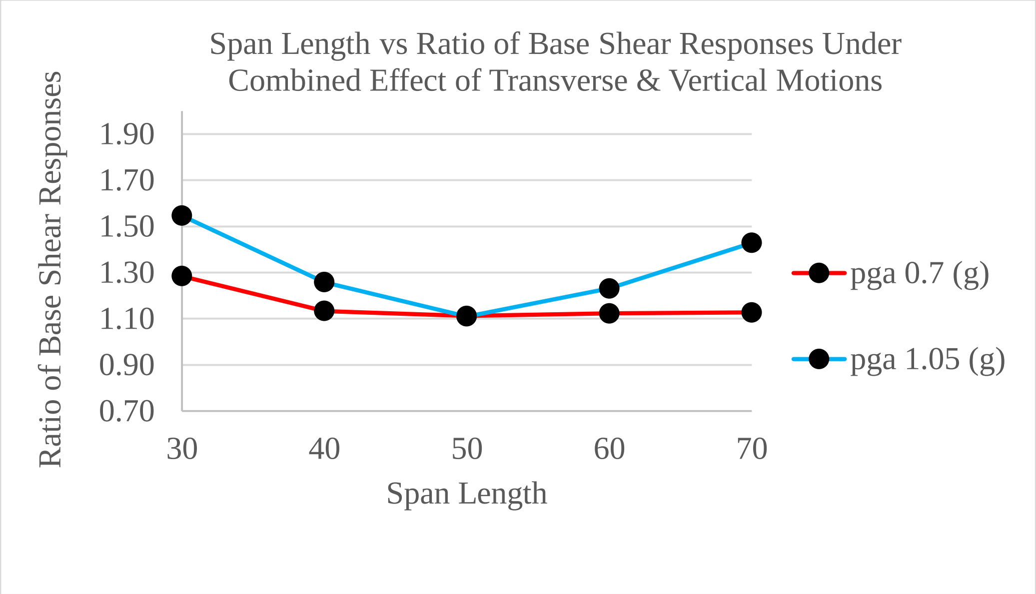

Figure 34. Span Length and Ratio of Base Shear Responses of Uplift-Restricted Case to Uplift-Allowed Case (Investigated Under the Combined Effect of Transverse and Vertical Motions Considering Two Different PGA values)

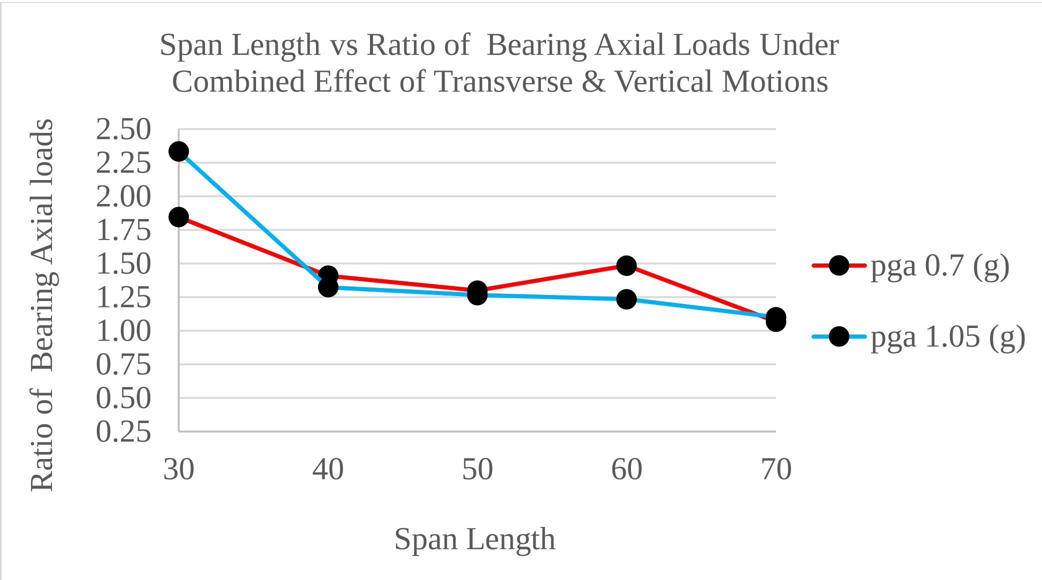

Figure 35. Span Length and Ratio of Bearing Axial Loads of Uplift-Restricted Case to Uplift-Allowed Case (Investigated Under the Combined Effect of Transverse and Vertical Motions Considering Two Different PGA values)

7.4 Comparison of Uplift-Allowed and Uplift-Restricted Bridge Models in Terms of Pier Height

This section is devoted to comparative assessment of the Uplift-Allowed bridge and Uplift-Restricted bridge with respect to bridge pier height. In order to investigate the effect of the bridge pier height on bridge superstructure rocking related seismic performance, 3 different quantities for bridge piers' height are considered namely 20, 30 and 40 meters. Although almost all of the bridges analyzed in this category show better seismic performance at their Uplift-Allowed case, the results of the analyses conducted for each pair of models under the effect of different peak ground acceleration levels of 0.7, 1.05 and 1.4 reveal that the effect of the rocking action decreases as the height of the bridge piers increases, the trends reflected at figures 36 and 37 for models under only transverse motion as well as trends obtained at figures 39 and 40 for models under Combined effect of transverse and vertical motions clearly indicate the superior performance of 20 meters tall Uplift-Allowed bridge model in comparison to the Uplift-Restricted bridge model of the same height.

7.4.1 Effect of Pier Height Investigated Under the Effect of Transverse Motion

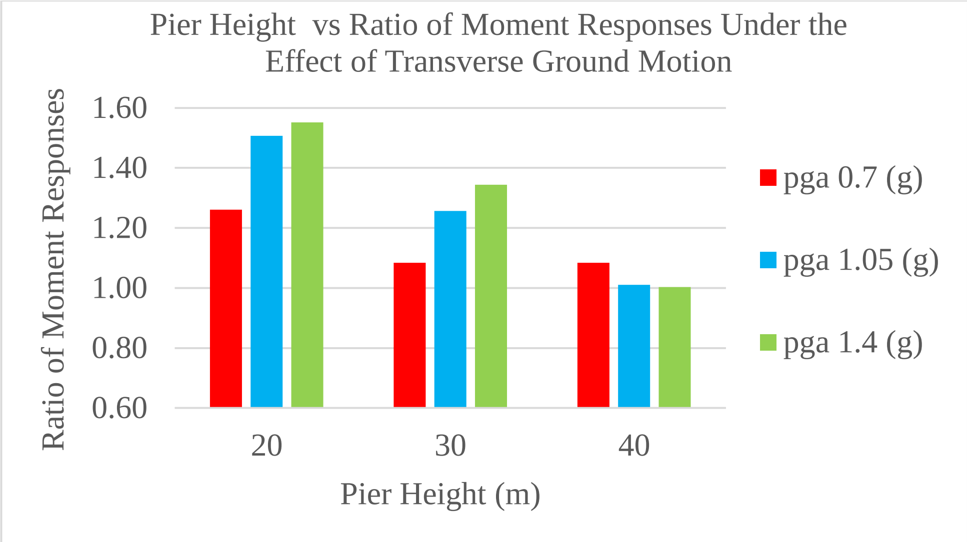

Figure 36. Pier Height and Ratio of Moment Responses of Uplift-Restricted Case to Uplift-Allowed Case (Investigated Under the Effect of Transverse Motion Considering Three Different PGA values)

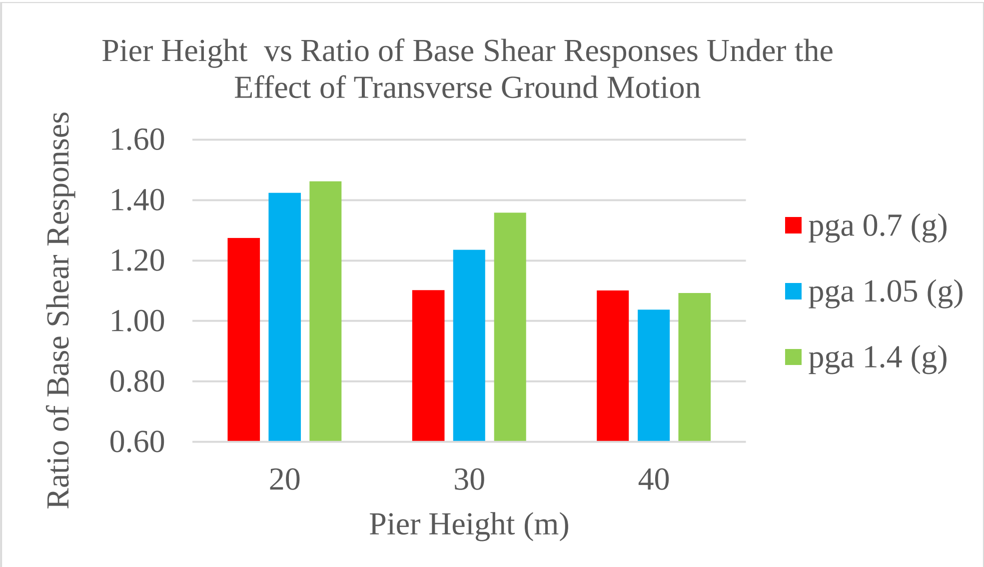

Figure 37. Pier Height and Ratio of Base Shear Responses of Uplift-Restricted Case to Uplift-Allowed Case (Investigated Under the Effect of Transverse Motion Considering Three Different PGA values)

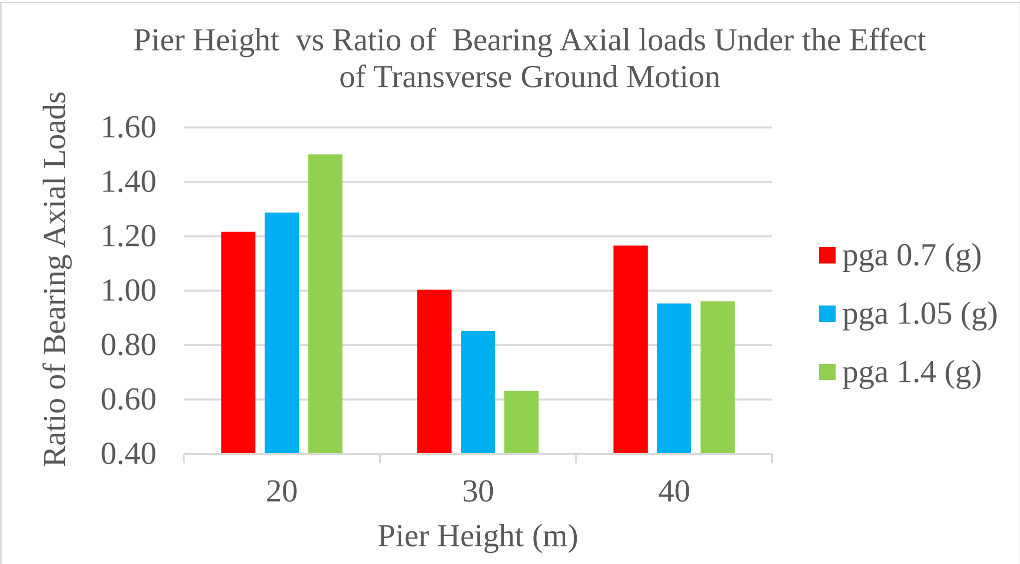

Figure 38. Pier Height and Ratio of Bearing Axial Loads of Uplift-Restricted Case to Uplift-Allowed Case (Investigated Under the Effect of Transverse Motion Considering Three Different PGA values)

7.4.2 Effect of Pier Height Investigated Under the Combined Effect of Transverse and Vertical Motions

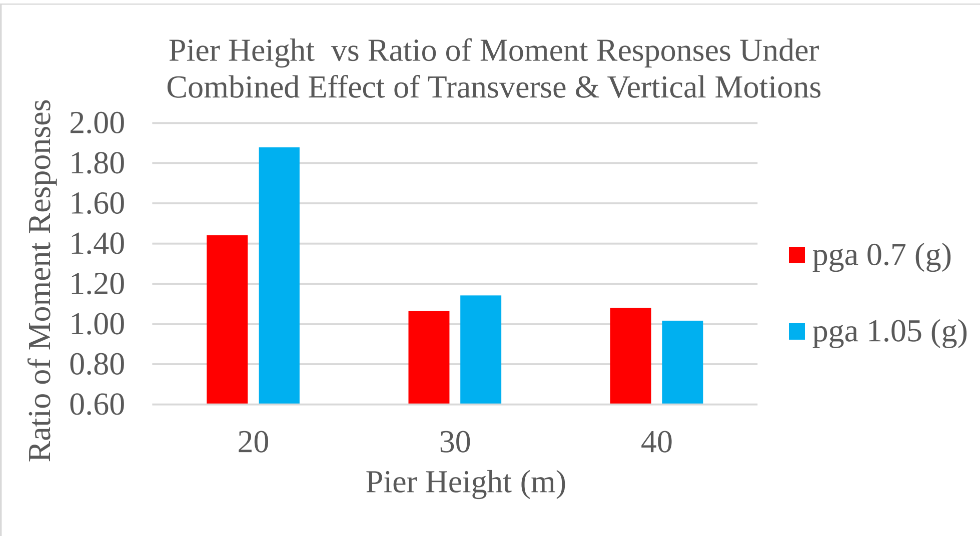

Figure 39. Pier Height and Ratio of Moment Responses of Uplift-Restricted Case to Uplift-Allowed Case (Investigated Under the Combined Effect of Transverse and Vertical Motions Considering Two Different PGA values)

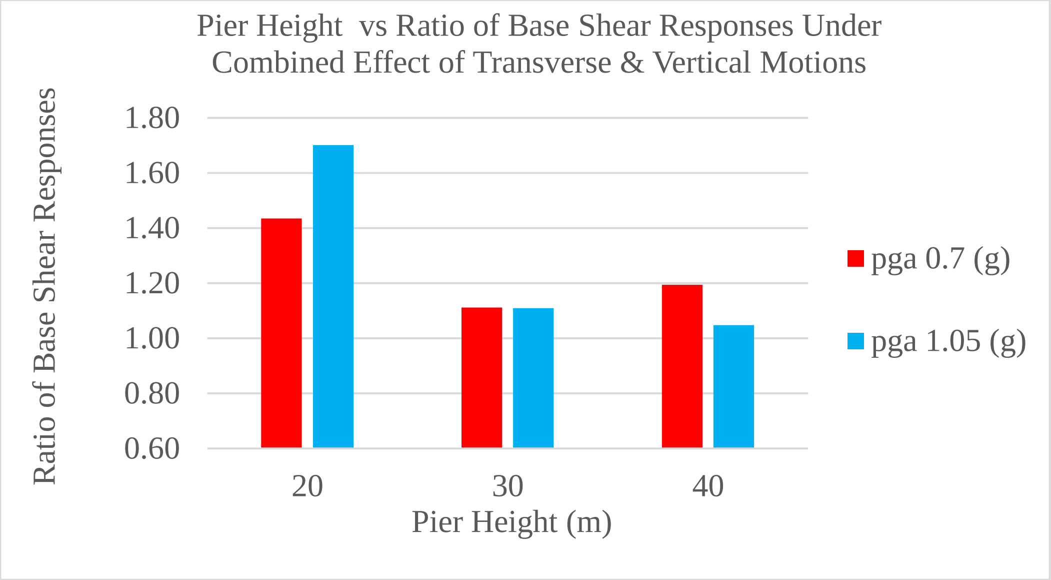

Figure 40. Pier Height and Ratio of Base Shear Responses of Uplift-Restricted Case to Uplift-Allowed Case (Investigated Under the Combined Effect of Transverse and Vertical Motions Considering Two Different PGA values)

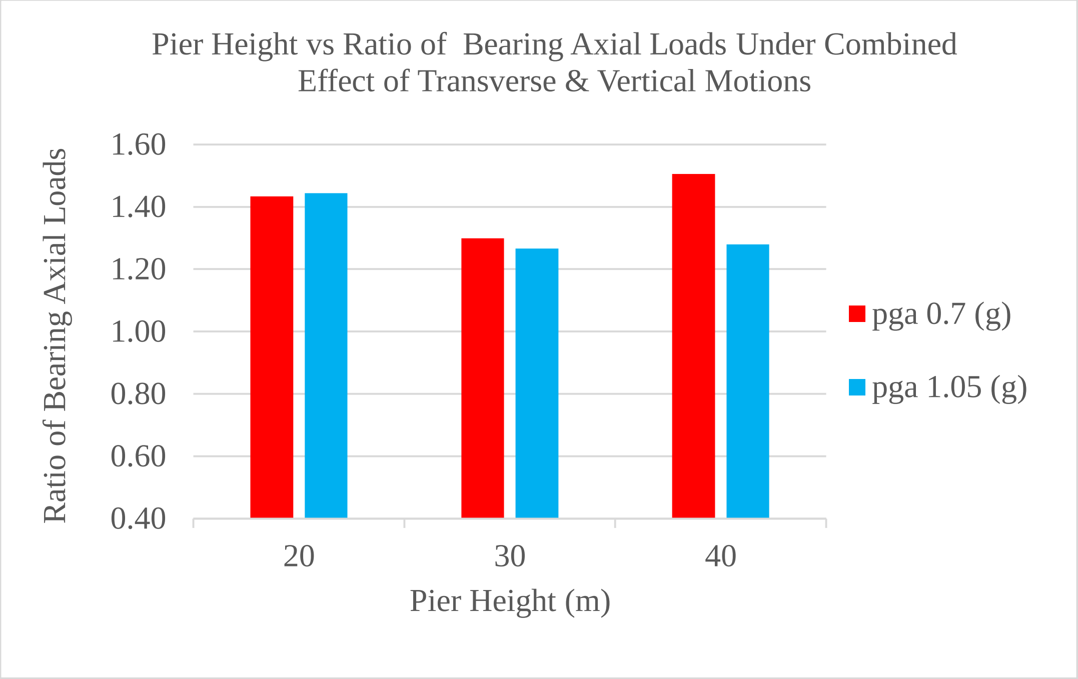

Figure 41. Pier Height and Ratio of Bearing Axial Loads of Uplift-Restricted Case to Uplift-Allowed Case (Investigated Under the Combined Effect of Transverse and Vertical Motions Considering Two Different PGA values)

7.5 Comparison of Uplift-Allowed and Uplift-Restricted Bridge Models in Terms of Friction coefficient of FPS System Isolators

In this Section, a comparative assessment of the Uplift-Allowed bridge and Uplift-Restricted bridge is discussed with respect to Friction Coefficient of Friction Pendulum Sliding (FPS) isolators. The values considered for investigation of effect of friction coefficient are 0.02, 0.03, 0.04, 0.05 and 0.06. The analyses results reveal that the pier moment and base shear responses of Uplift-Restricted bridges are larger than those of Uplift-Allowed ones regardless of value of friction coefficient used for FPS system isolators. However, the trends observed at figures 42 and 43 as well as 47 and 48 show that effect of the rocking actions decreases as the value of friction coefficient increases. Similarly the pattern shaped at figures 44 and 49 also show that the ratio of the axial load carried by Bearings at Uplift-Restricted bridge models to Uplift-Allowed models increases as the value of friction coefficient gets bigger which is a sign of correlation with previous figures in a sense that ,the more the rocking motion effect decreases, the level of axial load exerted to bearings of Uplift-Allowed case may be decreased which results in higher ratios of axially carried load at figures 44 and 49. The logic behind the explained behavior can be linked to higher horizontal forces being initiated at sliding bearings of bridge models with lower friction coefficient values like 0.02 than the models with bigger coefficient values which results in better superstructure rocking action to be initiated at models with smaller friction coefficient values.

7.5.1 Effect of Friction coefficient of FPS System Investigated Under the Effect of Transverse Motion

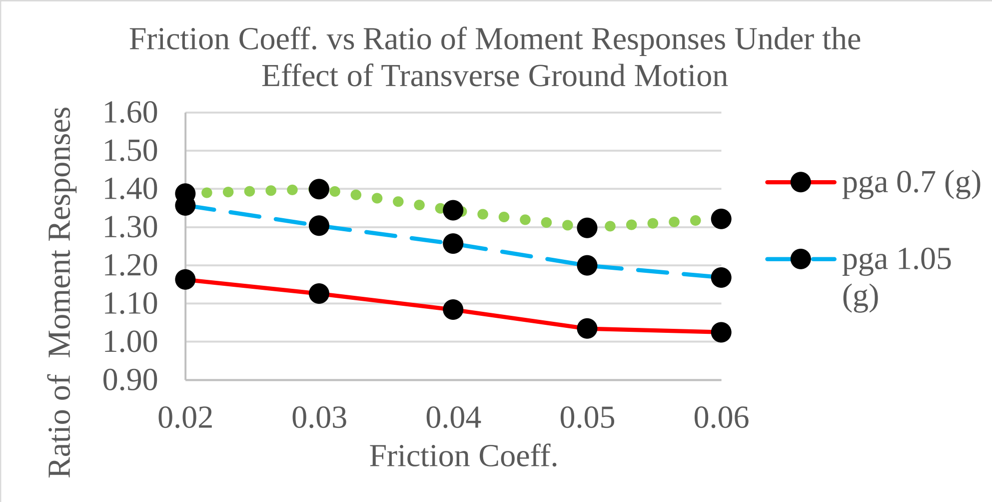

Figure 42. Friction Coefficient and Ratio of Moment Responses of Uplift-Restricted Case to Uplift-Allowed Case. (Investigated Under the Effect of Transverse Motion Considering Three Different PGA values)

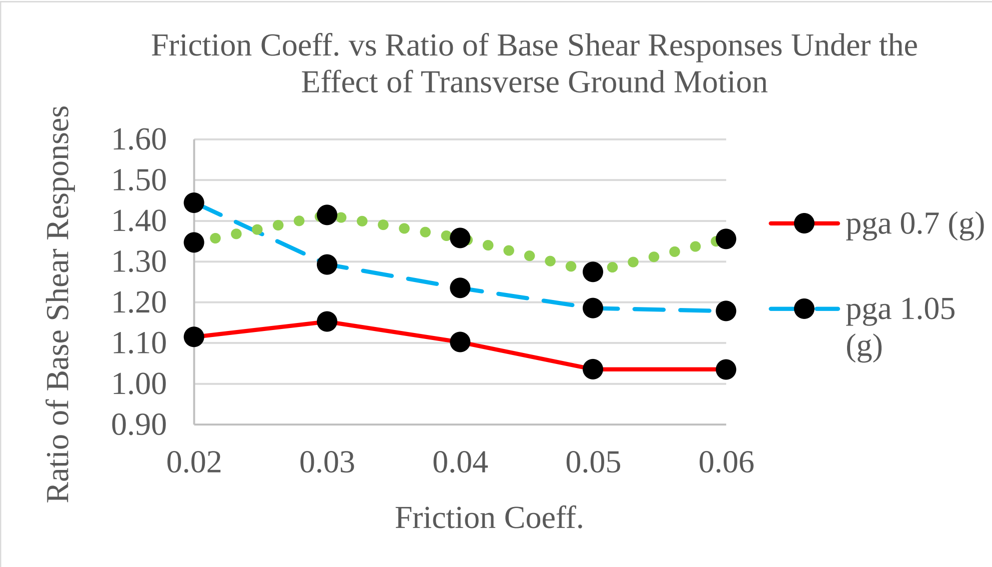

Figure 43. Friction Coefficient and Ratio of Base Shear Responses of Uplift-Restricted Case to Uplift-Allowed Case (Investigated Under the Effect of Transverse Motion Considering Three Different PGA values)

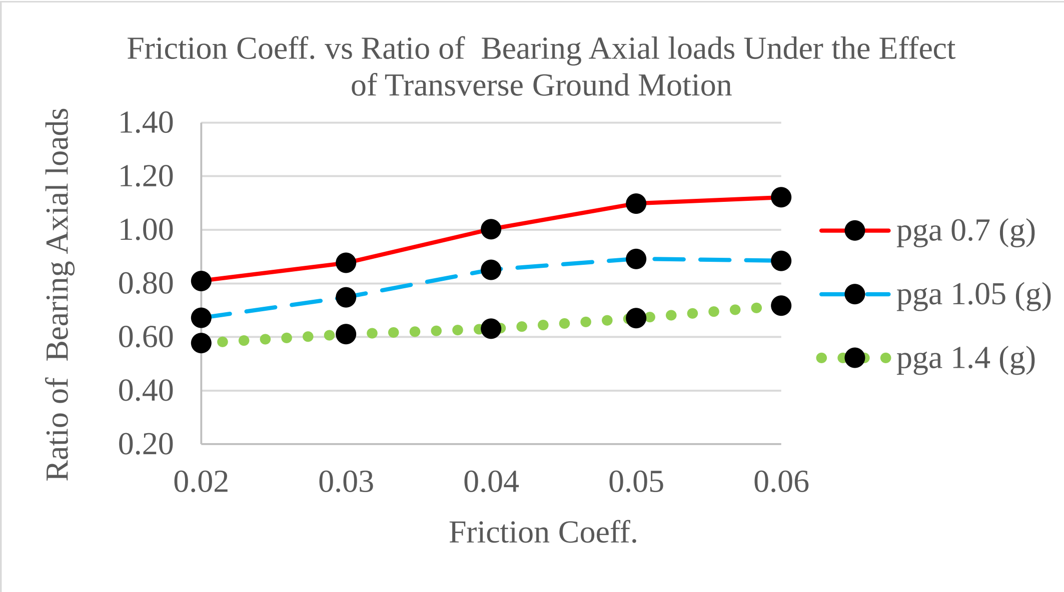

Figure 44. Friction Coefficient and Ratio of Bearing Axial Loads of Uplift-Restricted Case to Uplift-Allowed Case. (Investigated Under the Effect of Transverse Motion Considering Three Different PGA values)

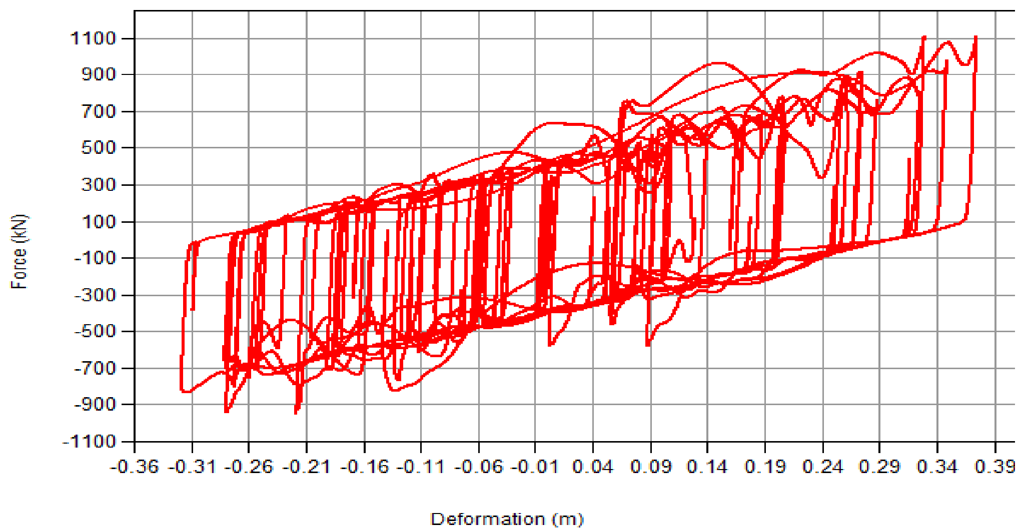

Figure 45. Force-Deformation Graph of FPS Isolator Having Friction Coefficient Equal to 0.06 Obtained Under RSN5778 Transverse Ground Motion with 1.05 (g) PGA

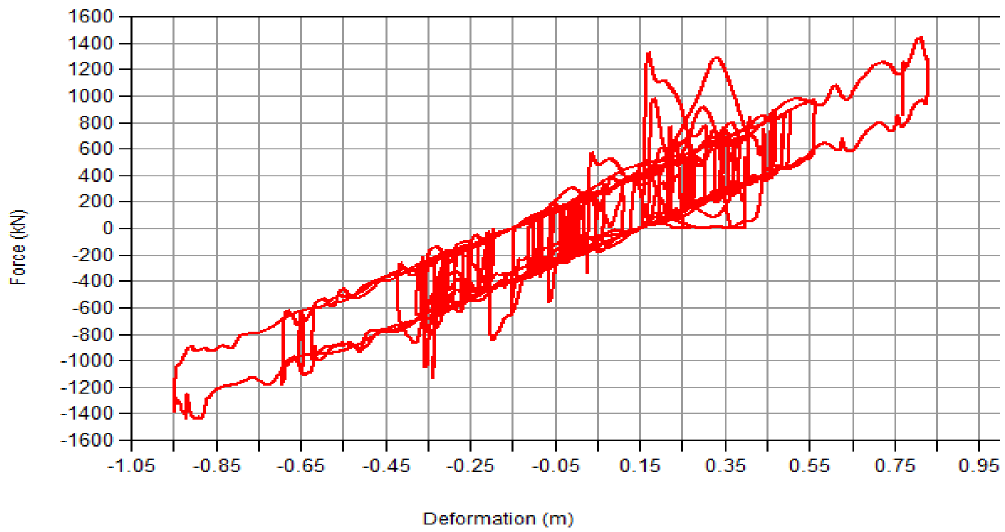

Figure 46. Force-Deformation Graph of FPS Isolator Having Friction Coefficient Equal to 0.02 Obtained Under RSN5778 Transverse Ground Motion with 1.05 (g) PGA

7.5.2 Effect of Friction coefficient of FPS System Investigated Under the Combined Effect of Transverse and Vertical Motions

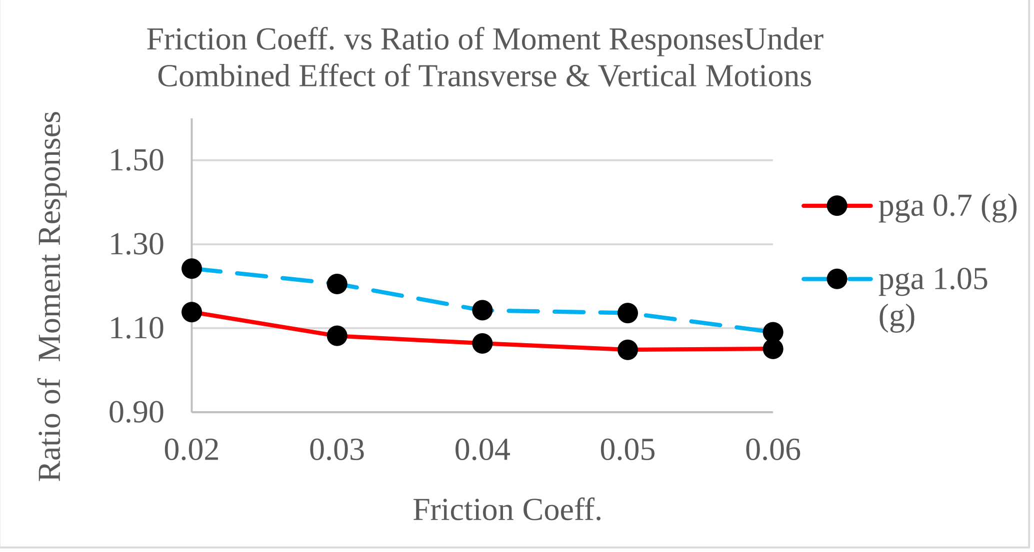

Figure 47. Friction Coefficient and Ratio of Moment Responses of Uplift-Restricted Case to Uplift-Allowed Case. (Investigated Under the Combined Effect of Transverse and Vertical Motions Considering Two Different PGA values)

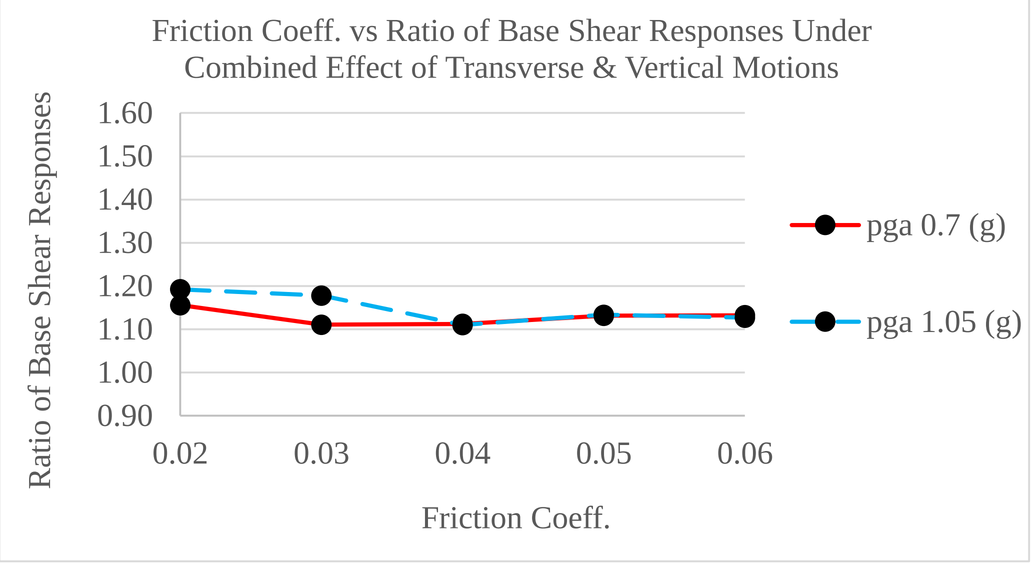

Figure 48. Friction Coefficient and Ratio of Base Shear Responses of Uplift-Restricted Case to Uplift-Allowed Case (Investigated Under the Combined Effect of Transverse and Vertical Motions Considering Two Different PGA values)

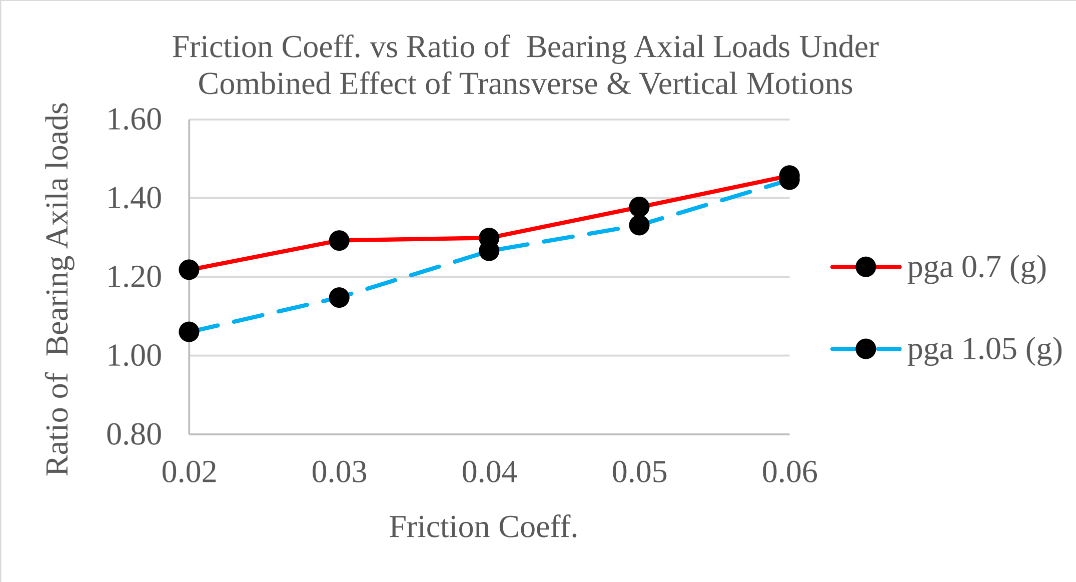

Figure 49. Friction Coefficient and Ratio of Bearing Axial Loads of Uplift-Restricted Case to Uplift-Allowed Case. (Investigated Under the Combined Effect of Transverse and Vertical Motions Considering Two Different PGA values)

7.6 Comparison of Uplift-Allowed and Uplift-Restricted Bridge Models in Terms of Radius of Curvature of FPS system

In this Section, a comparative assessment of Uplift-Allowed and Uplift-Restricted bridge is discussed with respect to radius of curvature of Friction Pendulum Sliding isolators. Values considered for investigation of effect of radius of curvature are 3, 4, 5, 6 and 7 (m). Each pair of Uplift-Restricted and Uplift-Allowed models are subjected to different levels of ground motion intensities specified by 0.7, 1.05 and 1.4 (g) peak ground acceleration values. Analyses conducted reveal that the pier moment and base shear responses of Uplift-Restricted bridge models are larger than Uplift-Allowed ones. At the same time by looking at the behavior reflected at figures 50 and 51 as well as 53 and 54, it can be clearly observed that the ratio of the responses at Uplift-Restricted cases to Uplift-Allowed ones do not change significantly and there is an steady pattern in this regard which shows that the factor having influence on performance of the Uplift-Allowed cases is only ground motion intensity factor and variation of radius of curvature value at friction pendulum system does not have much effect on the seismic behavior of bridge models.

7.6.1 Effect of Radius of Curvature of FPS System Investigated Under the Effect of Transverse Motion

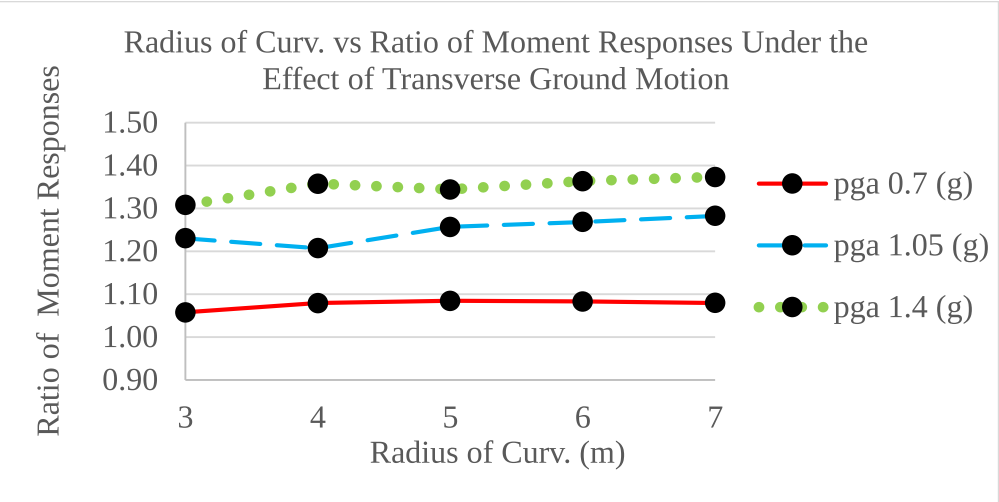

Figure 50. Radius of Curvature and Ratio of Moment Responses of Uplift-Restricted Bridge Model to Uplift-Allowed Case. (Investigated Under the Effect of Transverse Motion Considering Three Different PGA values)

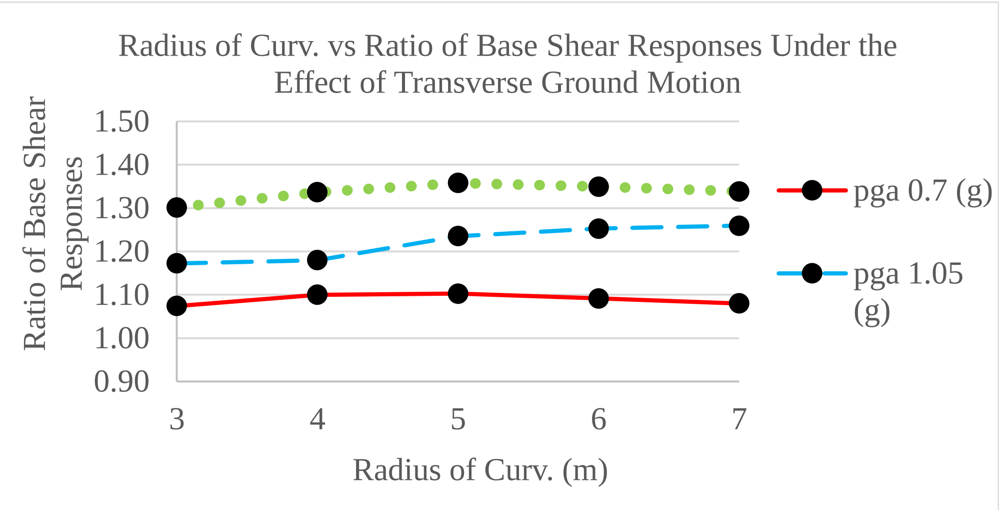

Figure 51. Radius of Curvature and Ratio of Base Shear Responses of Uplift-Restricted case to Uplift-Allowed Case (Investigated Under the Effect of Transverse Motion Considering Three Different PGA values)

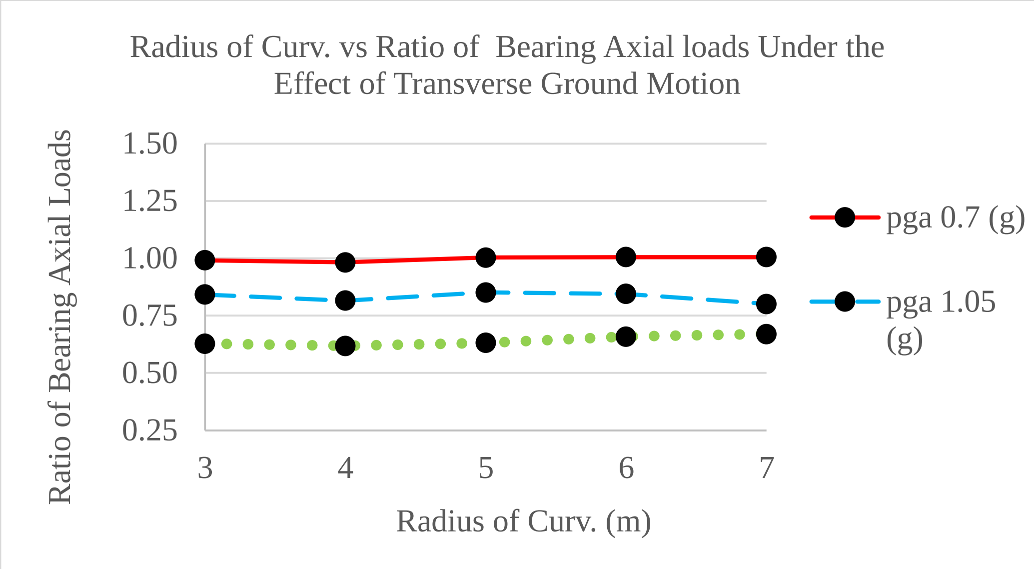

Figure 52. Radius of Curvature and Ratio of Bearing Axial Loads of Uplift-Restricted case to Uplift-Allowed case (Investigated Under the Effect of Transverse Motion Considering Three Different PGA values)

7.6.2 Effect of Radius of Curvature of FPS System Investigated Under the Combined Effect of Transverse and Vertical Motions

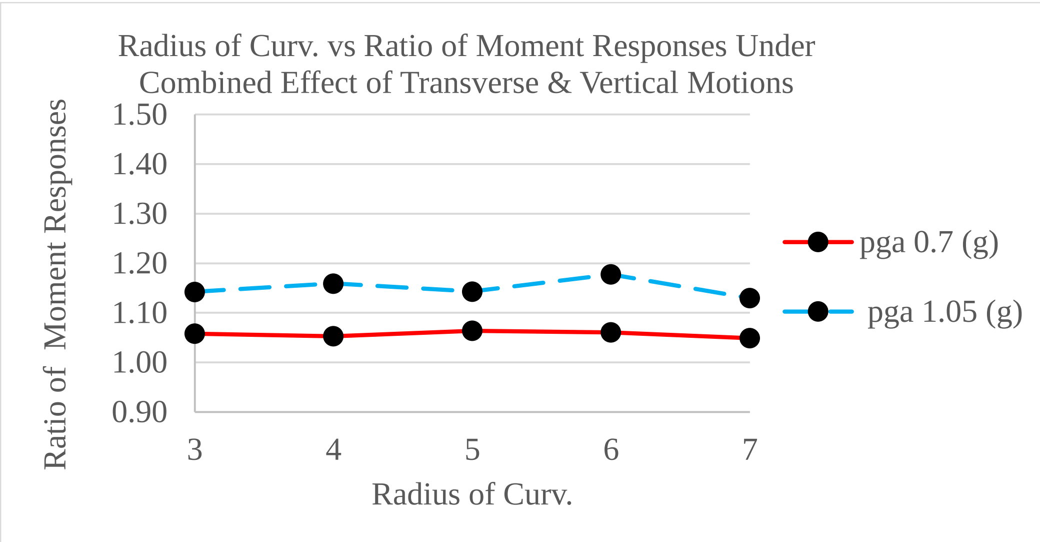

Figure 53. Radius of Curvature and Ratio of Moment Responses of Uplift-Restricted Bridge Model to Uplift-Allowed Case. (Investigated Under the Combined Effect of Transverse and Vertical Motions Considering Two Different PGA values)

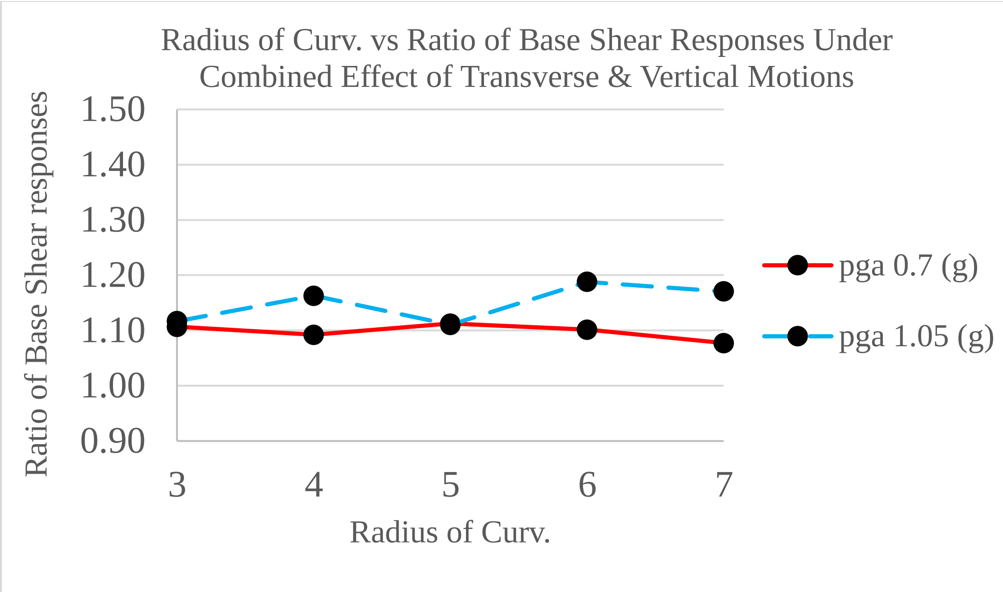

Figure 54. Radius of Curvature and Ratio of Base Shear Responses of Uplift-Restricted case to Uplift-Allowed Case (Investigated Under the Combined Effect of Transverse and Vertical Motions Considering Two Different PGA values)

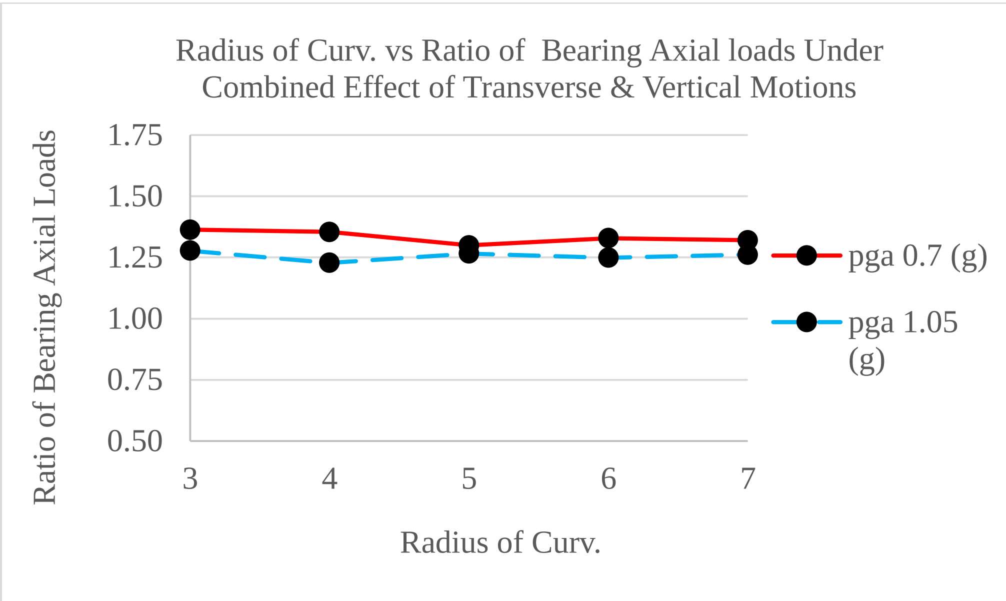

Figure 55. Radius of Curvature and Ratio of Bearing Axial Loads of Uplift-Restricted case to Uplift-Allowed case (Investigated Under the Combined Effect of Transverse and Vertical Motions Considering Two Different PGA values)

7.7 Comparison of Uplift-Allowed and Uplift-Restricted Bridge Models in Terms of Intensity of Ground Motion

In this Section, a comparative assessment of the Uplift-Allowed bridge and Uplift-Restricted bridge is discussed with respect to variation in intensity of ground motions. The section is divided for two parts accordingly. At first part, the seismic performance of Uplift-Allowed and Uplift-Restricted models are compared with each other only under transverse set of ground motions being applied in different levels of intensities determined by various PGA values. However, at second part in addition to transverse dynamic loads, there are also vertical dynamic loads applied simultaneously to bridge models to obtain a better idea about the behavior of bridge models and applicability of deck-rocking mechanism.

7.7.1 Effect of Intensity of Ground Motions Applied only in Transverse Direction

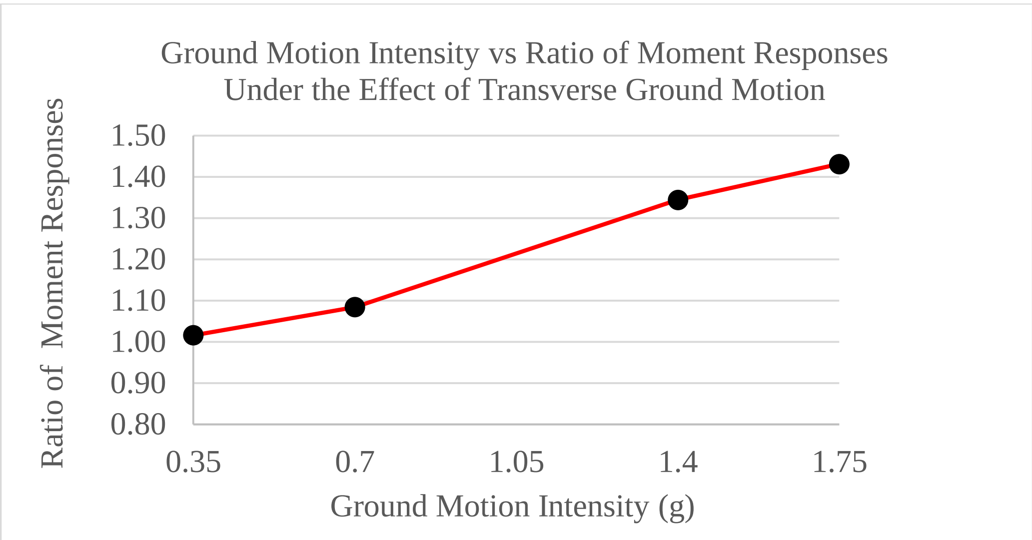

Figure 56. Ground Motion Intensity and Ratio of Moment Responses of Uplift-Restricted Case to Uplift-Allowed Case (Investigated Under the Effect of Transverse Motion)

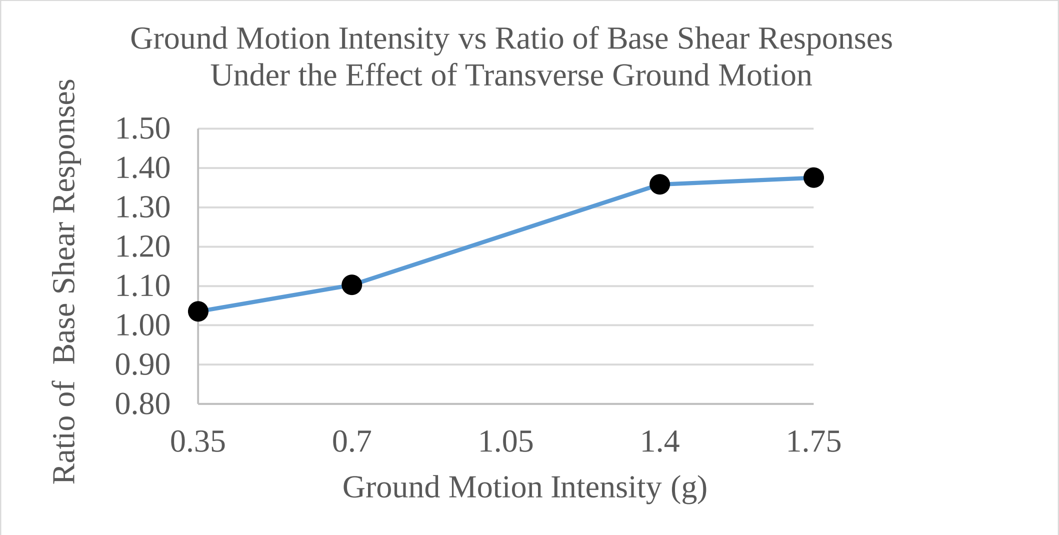

Figure 57. Ground Motion Intensity and Ratio of Base Shear Responses of Uplift-Restricted Case to Uplift-Allowed Case (Investigated Under the Effect of Transverse Motion)

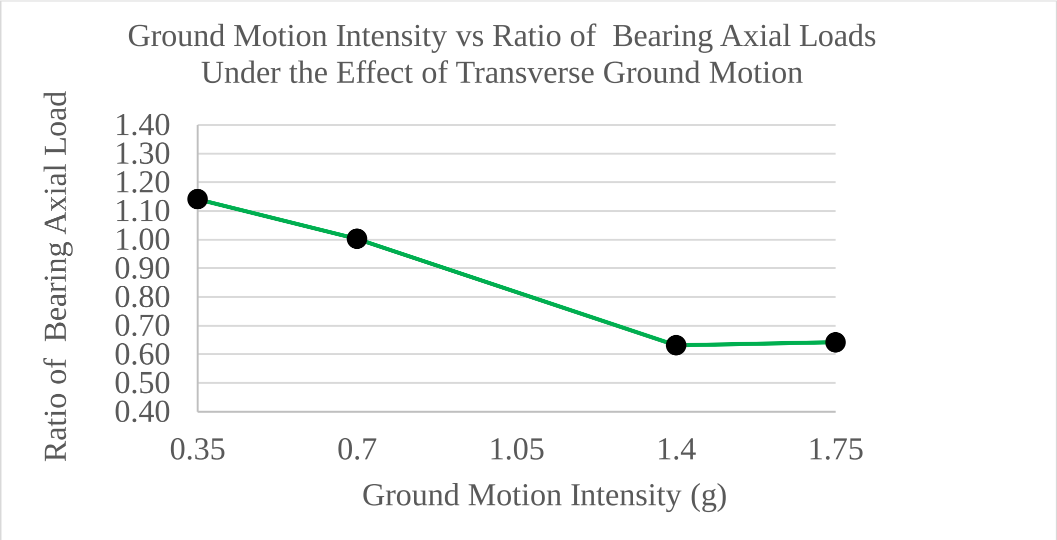

Figure 58. Ground Motion Intensity and Ratio of Bearing Axial Loads of Uplift-Restricted Case to Uplift-Allowed Case (Investigated Under the Effect of Transverse Motion)

The analyses results reveal that the pier moment and base shear responses of Uplift-Restricted bridges at each step get larger than those of Uplift-Allowed ones as the intensity of ground motions increases. By looking at Figures 56 and 57 , it can be clearly concluded that the deck rocking motion significantly improves the seismic behavior of bridge models at Uplift-Allowed bridge models under severe transverse motions. At the same time the trend obtained at figure 58 is also supporting the idea that, stronger rocking motion of the deck causes to FPS system isolators or bearings to tolerate more axial load in compression, which is related to physical characteristics of rocking block and the amount of dead load being transferred to opposite corners during rocking. In this case, the opposite sliding bearing.

7.7.2 Effect of Intensity of Ground Motions Applied in Transverse and Vertical Directions

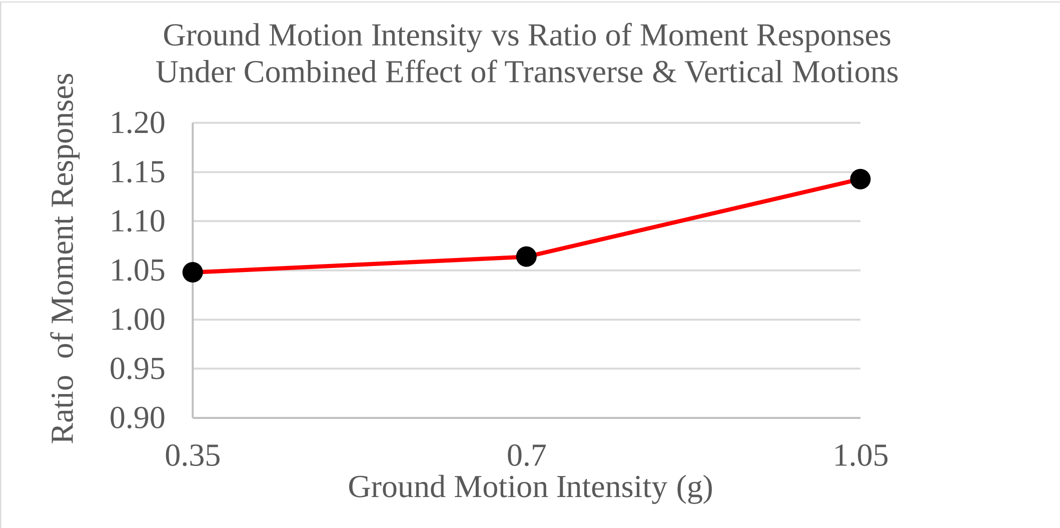

Figure 59.Ground Motion Intensity and Ratio of Moment Responses of Uplift-Restricted case to Uplift-Allowed Case (Investigated Under the Combined Effect of Transverse and Vertical Motions)

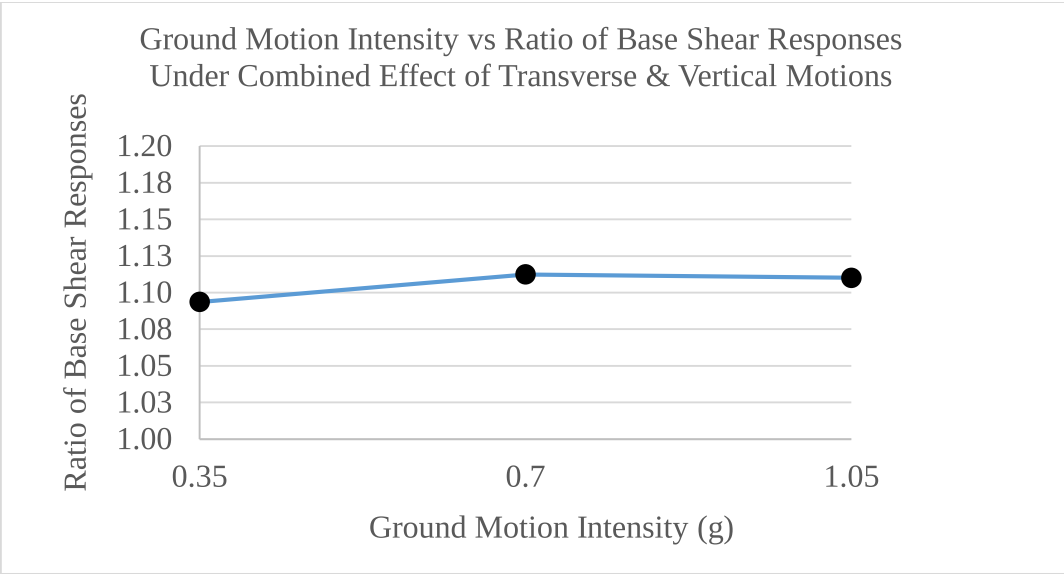

Figure 60. Ground Motion Intensity and Ratio of Base Shear Responses of Uplift-Restricted case to Uplift-Allowed case (Investigated Under the Combined Effect of Transverse and Vertical Motions)

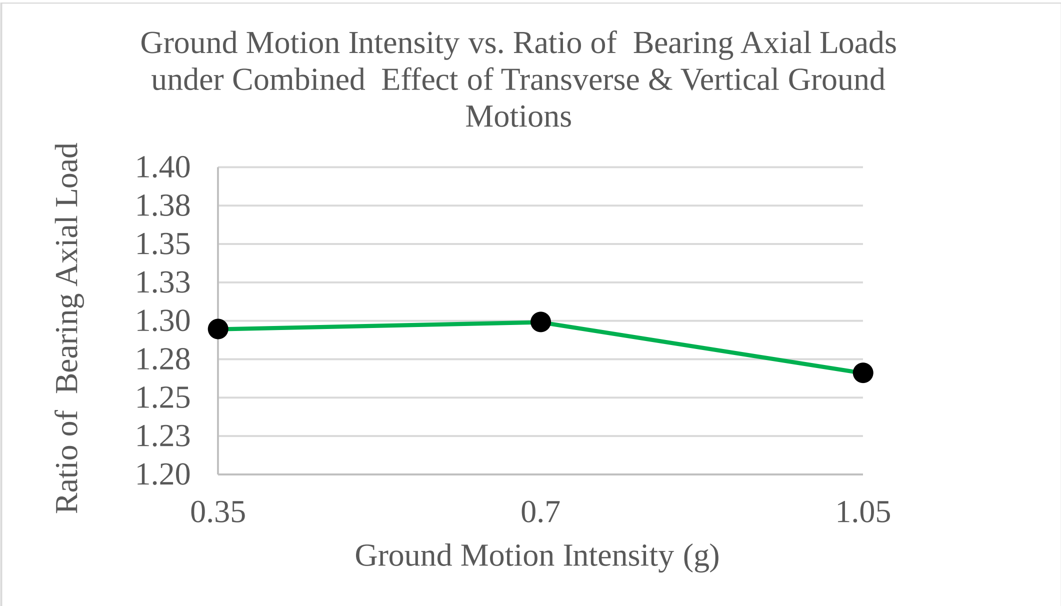

Figure 61. Ground Motion Intensity and Ratio of Bearing Axial Loads of Uplift-Restricted case to Uplift-Allowed case (Investigated Under the Combined Effect of Transverse and Vertical Motions)

The analyses results of second part also support the hypothesis of efficiency of rocking motion in improving the seismic performance of the structure but not that much apparent like previous case. The trends obtained at figures 59 and 60 also demonstrate that pier moment and base shear responses of Uplift-Restricted bridges get larger than those of Uplift-Allowed ones at higher ground motion intensity values. Another important point in regard to this case of combined transverse and vertical ground motion action is about maximum possible severity of ground motions. During the analysis of this case's bridge models, it was observed that upon 1.05 PGA values the Uplift-Allowed bridge models start to behave in opposite manner, showing decrease in their improved seismic response due to rocking, the reason for this may be attributed to stability related causes, which can possibly make the structure to be unstable under ground motion intensities with higher PGA values than 1.05 (g)

CHAPTER 8

CONCLUSION

The main goal in carrying out this study was to understand the effect of bridge deck rocking on the seimsic performance of box girder type of bridges and in doing so, a comparative based approach under different seismic intensity levels determined by various peak ground acclerations was followed. Altohough the findigns are specific to the models taken into account in this study, it should be noted that the similar perfomrance is expected in all multiple-span bridges chosen in this study. In general, Uplift-Allowed bridges in the study showed better seismic performance compared to Uplift-Restridted ones as the value of the peak ground acceleration increased in the analyses. This can be mainly attributed to the level of energy being damped out due to kinetic motion of supersturcute deck and existence of fictisious dampers in connection phase of superstructure with substructure resembling contact-related effect of rigid bodies' collision. In the case of Uplift-Restricted bridge models, the superstructure is supported by FPS isolators only to have horizontal translation during an earthquake action. This type of structural configuration leads to produce larger base shear and moment repsonses compared to that of Uplift-Allowed bridges where the superstructure deck is allowed to freely rock and as a result, absorb part of seismically initiated energy. In terms of axial loads being carried by sliding bearings, it was observed that at majority of the bridge models, the amount of axial load exerted on bearings increases as a result of the superstructure rocking which as an expected behavior is sign of accuracy of rigid block rocking theory discussed in depth in the study. Surprisingly, the rocking action observed to show lower efficiancy as the value of FPS friction coefficient got bigger during the analysis which is linked to smaller forces initiated at bearings with bigger isolation system friction coefficient value. Although the value of friction coefficient has a direct relation with horizontally initiated force at FPS bearings but at the same time, the more the value of friction coefficinet increases, the more the degree of deck diplacement decreases and this oppositely affects the amount of horizontal Force value of FPS bearings which in the current study leads to greater seismic repsonses at lower values of frcition coefficinet as physical parameter used in design of sliding bearings. In summary, it can be concluded that Uplift-Allowed bridges have superior seismic performance in terms of smaller pier moment and base shear responses compared to Uplift-Restricted bridges in majority of models designed for this study.

REFERENCES

1. AASHTO Guide Specification for Seismic Isolation Design, (2014), Washington
2. AASHTO (2010) Load and resistance factor design (LRFD) specifications. AASHTO, Washington
3. Agalianos, A., Psychari, A., Vassiliou, M. F., Stojadinovic, B., & Anastasopoulos, I. (2017). Comparative assessment of two rocking isolation techniques for a motorway overpass bridge. Frontiers in Built Environment, 3, 47.
4. Amirzehni, E., Taiebat, M., Finn, W. L., & DeVall, R. H. (2015). Ground Motion Scaling/matching for Nonlinear Dynamic Analysis of Basement Walls. In The 11th Canadian Conference on Earthquake Engineering.
5. Anagnostopoulos, S. A. (1988). Pounding of buildings in series during earthquakes. Earthquake engineering & structural dynamics, 16(3), 443-456.
6. Anastasopoulos, I., Gazetas, G., Loli, M., Apostolou, M., & Gerolymos, N. (2010). Soil failure can be used for seismic protection of structures. Bulletin of Earthquake Engineering, 8(2), 309-326.
7. Antonellis, G., Gavras, A. G., Panagiotou, M., Kutter, B. L., Guerrini, G., Sander, A. C., & Fox, P. J. (2015). Shake table test of large-scale bridge columns supported on rocking shallow foundations. Journal of Geotechnical and Geoenvironmental Engineering, 141(5), 04015009.
8. ASCE. (2003, September). Seismic evaluation of existing buildings. American Society of Civil Engineers.
9. Barros, R. C., Naderpour, H., Khatami, S. M., & Mortezaei, A. (2013). Influence of seismic pounding on RC buildings with and without base isolation system subject to near-fault ground motions. Journal of Rehabilitation in Civil Engineering, 1(1), 39-52.

10. Beck, J. L., & Skinner, R. I. (1973). The seismic response of a reinforced concrete bridge pier designed to step. Earthquake Engineering & Structural Dynamics, 2(4), 343-358.
11. Calvi, G., Palermo, A. G., & Pampanin, S. (2005). Use of" controlled rocking" in the seismic design of bridges. In proceedings of the 13th world conference on earthquake engineering 13 WCEE (pp. 1-16).
12. Chen, Y. H., Liao, W. H., Lee, C. L., & Wang, Y. P. (2006). Seismic isolation of viaduct piers by means of a rocking mechanism. Earthquake engineering & structural dynamics, 35(6), 713-736.
13. Cheng, C. T. (2008). Shaking table tests of a self-centering designed bridge substructure. Engineering Structures, 30(12), 3426-3433.
14. Cheok, G. S. (1997). A hybrid reinforced precast frame for seismic regions. PCI journal, 42(2), 20-32.
15. Dicleli, M., Lee, J. Y., & Mansour, M. (2004, August). Importance of soil-bridge interaction modeling in seismic analysis of seismic-isolated bridges. In Proceedings of 13th world conference on earthquake engineering, Vancouver, BC, Canada, paper (No. 3147).
16. Fang, H. Y. (2013). Foundation engineering handbook. Springer Science & Business Media.
17. Gajan, S., & Kutter, B. L. (2008). Capacity, settlement, and energy dissipation of shallow footings subjected to rocking. Journal of Geotechnical and Geoenvironmental Engineering, 134(8), 1129-1141.
18. Gajan, S., & Saravanathiiban, D. S. (2011). Modeling of energy dissipation in structural devices and foundation soil during seismic loading. Soil Dynamics and Earthquake Engineering, 31(8), 1106-1122.
19. Gazetas, G. (1991). Foundation vibrations. In Foundation engineering handbook (pp. 553-593). Springer, Boston, MA.
20. Gelagoti, F., Kourkoulis, R., Anastasopoulos, I., & Gazetas, G. (2012). Rocking-isolated frame structures: Margins of safety against toppling

collapse and simplified design approach. Soil Dynamics and Earthquake Engineering, 32(1), 87-102.

21. Giouvanidis, A. I., & Dimitrakopoulos, E. G. (2017). Seismic performance of rocking frames with flag-shaped hysteretic behavior. Journal of Engineering Mechanics, 143(5), 04017008.
22. Housner, G. W. (1963). The behavior of inverted pendulum structures during earthquakes. Bulletin of the seismological society of America, 53(2), 403-417.
23. Jankowski, R., & Mahmoud, S. (2015). Earthquake-induced structural pounding. Cham: Springer International Publishing.
24. Kalliontzis, D., & Sritharan, S. (2020). Dynamic response and impact energy loss in controlled rocking members. Earthquake Engineering & Structural Dynamics, 49(4), 319-338.
25. Khatami, S. M., Naderpour, H., Barros, R. C., Jakubczyk-Gałczyńska, A., & Jankowski, R. (2019). Effective formula for impact damping ratio for simulation of earthquake-induced structural pounding. Geosciences, 9(8), 347.
26. Liu, R., & Palermo, A. (2016). Pier to deck interaction and robustness of PRESSS hybrid rocking: issues affecting hammerhead pier bridges. In Proceedings, New Zealand Society for Earthquake Engineering 2016 Conference.
27. Makris, N. (2014). A half-century of rocking isolation. Earthquakes and Structures, 7(6), 1187-1221.
28. Makris, N., & Vassiliou, M. F. (2015). Dynamics of the rocking frame with vertical restrainers. Journal of Structural Engineering, 141(10), 04014245.
29. Mander, J. B., & Cheng, C. T. (1997). Seismic resistance of bridge piers based on damage avoidance design. In Seismic resistance of bridge piers based on damage avoidance design (pp. 109-109).
30. Marriott, D., Pampanin, S., & Palermo, A. (2009). Quasi-static and pseudo-dynamic testing of unbonded post-tensioned rocking bridge piers with

external replaceable dissipaters. Earthquake engineering & structural dynamics, 38(3), 331-354.

31. Medina, R., & Krawinkler, H. (2004). Pacific Earthquake Engineering Research Center. University of California, Berkeley.
32. Mergos, P. E., & Kawashima, K. (2005). Rocking isolation of a typical bridge pier on spread foundation. Journal of Earthquake Engineering, 9(sup2), 395-414.
33. Naeim, F., Alimoradi, A., & Pezeshk, S. (2004). Selection and scaling of ground motion time histories for structural design using genetic algorithms. Earthquake spectra, 20(2), 413-426.
34. Pelekis, I., Madabhushi, G. S., & DeJong, M. J. (2017, January). A centrifuge investigation of two different soil-structure systems with rocking and sliding on dense sand. In 6th ECCOMAS thematic conference on computational methods in structural dynamics and earthquake engineering, Rhodes Island Greece. European community on computational methods in applied sciences, Barcelona.
35. Plaut, R. H., Fielder, W. T., & Virgin, L. N. (1996). Fractal behavior of an asymmetric rigid block overturning due to harmonic motion of a tilted foundation. Chaos, Solitons & Fractals, 7(2), 177-196.
36. Priestley, M. N., Sritharan, S., Conley, J. R., & Pampanin, S. (1999). Preliminary results and conclusions from the PRESSS five-story precast concrete test building. PCI journal, 44(6), 42-67.
37. Psycharis, I. N., & Jennings, P. C. (1983). Rocking of slender rigid bodies allowed to uplift. Earthquake engineering & structural dynamics, 11(1), 57-76.
38. Routledge, P. J., Cowan, M. J., & Palermo, A. (2016). Low-damage detailing for bridges—a case study of Wigram–Magdala bridge. In Proceedings, New Zealand society for earthquake engineering 2016 conference. Christchurch.

39. Shrestha, B., Hao, H., & Bi, K. (2017). Devices for protecting bridge superstructure from pounding and unseating damages: an overview. Structure and Infrastructure Engineering, 13(3), 313-330.
40. Vassiliou, M. F., & Makris, N. (2015). Dynamics of the vertically restrained rocking column. Journal of Engineering Mechanics, 141(12), 04015049.
41. Yim, C. S., Chopra, A. K., & Penzien, J. (1980). Rocking response of rigid blocks to earthquakes. Earthquake Engineering & Structural Dynamics, 8(6), 565-587.
42. Zhang, J., & Makris, N. (2001). Rocking response of free-standing blocks under cycloidal pulses. Journal of Engineering Mechanics, 127(5), 473